

Fig. 2. Phagocytosis is a first signal for mSP1000-induced IL-1 β production. (A) Involvement of phagocytosis in mSP1000-induced IL-1 β production. PMA-primed THP-1 cells were treated with mSP1000s or ATP for 6 h in the absence (black bars) or presence (white bars) of cytochalasin D (5 μ M). IL-1 β production levels were then measured by ELISA. Data represent means \pm SD ($n=5$; * $P < 0.05$, ** $P < 0.01$ versus value for cytochalasin D [-] control within each treatment pair, t -test). (B) TEM analysis of mSP1000s. PMA-primed THP-1 cells were treated with mSP1000s for 6 h. Cells were then observed by TEM. Arrows indicate ingested mSP1000s. (C) Flow cytometry of FITC-mSP1000s taken up into PMA-primed THP-1 cells. Cells were treated with mSP1000s and incubated for 6 h at 37 $^{\circ}$ C (left) or 4 $^{\circ}$ C (right). Data were analyzed by using the FL-1 parameter for green fluorescence.

treated the cells with mSP1000s or ATP, a well-known caspase-1 activator without cellular internalization. The cytochalasin D abolished the mSP1000-induced IL-1 β production, whereas the response to ATP was unaffected (Fig. 2A). These results indicate that cellular ingestion of mSP1000s might be the first signal in the

inflammatory response. We then speculated that the reduction in IL-1 β production through surface modification of mSP1000s resulted from a change in the particle uptake frequency. We used TEM and flow cytometry to evaluate the frequency of uptake of mSP1000s (Fig. 2B, C). TEM analysis clearly showed that both the modified and unmodified mSP1000s were taken up by THP-1 cells (Fig. 2B). Furthermore, flow-cytometric analysis using FITC-conjugated mSP1000s showed that the frequencies of cellular ingestion of modified and unmodified mSP1000s were comparable at 37 $^{\circ}$ C (Fig. 2C). We also noted that the intensity of FITC-derived fluorescence was almost the same among the different types of mSP1000, and that the increase in the FL-1 signals was dose dependent (data not shown). These results collectively indicate that the unmodified and surface-modified mSP1000s were taken up with similar frequencies equally into the THP-1 cells by actin-dependent phagocytosis, independent of the type of modification group. Therefore, we considered that the difference in IL-1 β production levels among mSP1000s was resulted from the signaling intensity in the IL-1 β production cascade after ingestion of the mSP1000s by the cell.

3.3. Activation of caspase-1 by mSP1000s

IL-1 β production is regulated by pro-IL-1 β mRNA expression levels and by caspase-1 activity [17,22,23]. Therefore, to examine the mechanisms of the reduction in IL-1 β production by surface modification, we used semi-quantitative RT-PCR to investigate the expression levels of pro-IL-1 β mRNA in THP-1 cells treated with each type of mSP1000 (Fig. 3A). There were no significant differences in the expression levels of pro-IL-1 β mRNA between cells treated with unmodified and modified mSP1000s. We then tested whether the reduction in IL-1 β production by surface modification of mSP1000s resulted from changes in caspase-1 activity induced by mSP1000s. To investigate the association of caspase-1 activity with mSP1000-induced IL-1 β production, we treated cells with mSP1000s in the presence of a caspase-1 specific inhibitor, zVAD-fmk, and analyzed the IL-1 β production levels (Fig. 3B). The results showed that zVAD-fmk almost completely abrogated the IL-1 β production induced by mSP1000s. These results collectively indicate that the IL-1 β production induced by unmodified mSP1000 depend on the activation of caspase-1. Furthermore, it was speculated that the surface-modified mSP1000s induced little caspase-1 activation.

3.4. Activation of NLRP3 inflammasome by unmodified mSP1000

Recently, NLRP3 inflammasome was identified as the principal activator of caspase-1 in response to several types of danger signal [17,22,23]. To examine whether unmodified mSP1000 exerts their inflammatory potential through NLRP3 inflammasome, we examined the activation of NLRP3 inflammasome on THP-1 cells after treatment with unmodified mSP1000 (Fig. 4) [13,23]. We transiently transfected THP-1 cells with a plasmid expressing CFP-ASC fusion protein. ASC forms large oligomers after its activation, and the clustering of CFP-ASC can be used as an "optical reporter" of the activation of NLRP3 inflammasome [25,30]. Under baseline conditions CFP-ASC fluorescence was evenly distributed in the cytoplasm. Four hours after treatment with unmodified mSP1000, we detected bright fluorescent clusters of CFP-ASC in the cytoplasm. These clusters were not detected in non-transfected THP-1 cells treated with unmodified mSP1000, indicating that the clusters represented cytoplasmic aggregates of activated ASC in NLRP3 inflammasome. These results indicate that mSP1000-induced IL-1 β production is mediated by the activation of NLRP3 inflammasome.

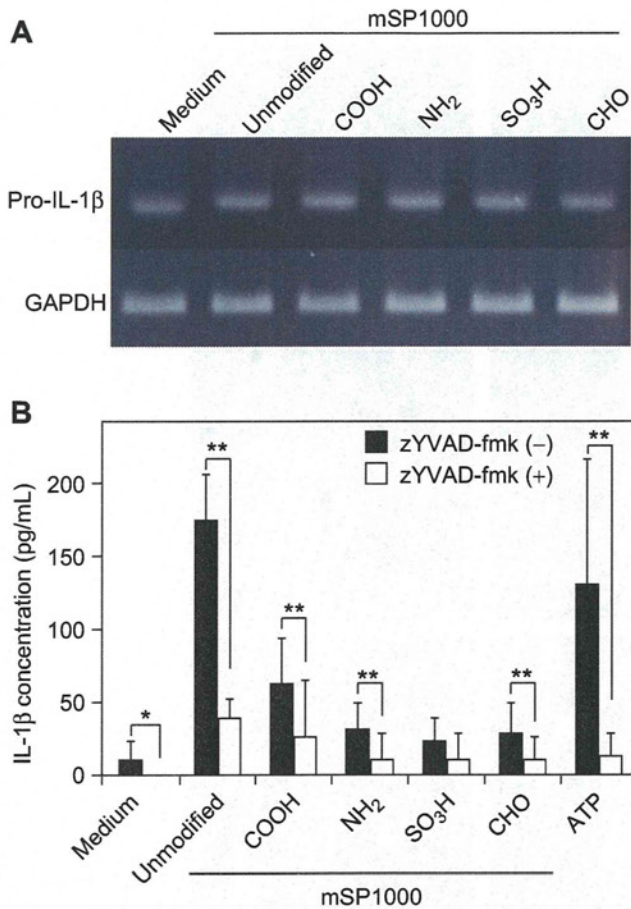


Fig. 3. Differences in levels of IL-1 β production induced by each type of mSP1000 depend on caspase-1 activation. (A) Pro-IL-1 β mRNA expression levels in mSP1000-treated cells. PMA-primed THP-1 cells were treated with mSP1000s and incubated for 3 h. Then, total RNA was isolated, and RT-PCR was performed with primers specific for IL-1 β (top) or GAPDH (bottom). (B) Involvement of caspase-1 activity in mSP1000-induced IL-1 β production. PMA-primed THP-1 cells were treated with each type of mSP1000 or with ATP for 6 h in the absence (black bars) or presence (white bars) of zYVAD-fmk (10 μ M). IL-1 β production levels were analyzed by ELISA. Data represent means \pm SD ($n = 5$; * $P < 0.05$, ** $P < 0.01$ versus value for zYVAD-fmk [-] control within each treatment pair, t -test).

3.5. Endosomal rupture and cathepsin B leakage

With crystalline silica, Hornung et al. reported that endosomal rupture plays a central role in activation of NLRP3 inflammasome followed by leakage of cathepsin B, an endosomal hydrolytic enzyme [20]. To investigate the mechanisms of IL-1 β production induced by mSP1000, we compared the frequency of endosomal rupture and subsequent cathepsin B leakage among each type of mSP1000, using Alexa Fluor 594 dextran as an endocytic compartment marker [31]. Mature endosomes incorporating dextran are observed as dotted forms, and the spread of dextran into the cytoplasm is recognized as an indicator of endosomal rupture [20]. We incubated THP-1 cells with dextran and different types of mSP1000 and observed the behavior of the ingested dextran by confocal microscopy (Fig. 5A). Upon treatment of the cells with unmodified mSP1000, we detected the obvious spread of dextran throughout the cytosol, unlike in untreated control cells, indicating that unmodified mSP1000 induced endosomal rupture (Fig. 5A). In contrast, the degree of endosomal rupture was decreased in cells treated with surface-modified mSP1000s, while mSP1000-COOH

induced endosomal rupture to some extent as the IL-1 β production levels (Fig. 5A). To investigate whether cathepsin B was involved in mSP1000-induced IL-1 β production, we treated cells with mSP1000s in the presence of a specific inhibitor of vacuolar H⁺-ATPase (bafilomycin A₁), which is needed to activate cathepsin B and a membrane-permeable cathepsin B-specific chemical inhibitor (CA-074-Me). Both inhibitors almost completely suppressed IL-1 β production induced by mSP1000s (Fig. 5B and C). These results collectively suggest that the activation of NLRP3 inflammasome and subsequent IL-1 β production induced by mSP1000s are triggered by active cathepsin B leakage into the cytoplasm. Furthermore, they suggest that the reduction in IL-1 β production by surface modification of mSP1000s results from a reduction in the frequency of mSP1000-induced endosomal rupture and subsequent cathepsin B leakage.

3.6. ROS production of mSP1000s

Another study has shown that ROS, in addition to cathepsin B, plays a crucial role in NLRP3 activation [13,19]. To investigate whether mSP1000-induced activation of NLRP3 inflammasome is dependent on ROS, we measured the levels of ROS in mSP1000-treated THP-1 cells by H₂DCFDA [32]. Treatment of THP-1 cells with unmodified mSP1000, but not with surface-modified SP1000s, significantly enhanced ROS production compared with that in the medium control (Fig. 6A). To confirm the involvement of ROS in mSP1000-induced IL-1 β production, we evaluated the levels of IL-1 β induced by mSP1000s in the presence of a broad ROS scavenger, BHA, or a specific inhibitor of NADPH oxidase, DPI. NADPH oxidase is an important enzymatic source for the production of ROS [33]. We confirmed that both BHA and DPI significantly suppressed unmodified mSP1000-induced IL-1 β production (Fig. 6B and C). These results indicate that, in addition to cathepsin B, mSP1000-induced ROS play an important role in NLRP3 activation.

We then examined the association between mSP1000-induced ROS production and endosomal rupture. We incubated cells with dextran and unmodified mSP1000 in the presence of BHA and observed the behavior of the dextran as a reflection of endosomal morphology. The endosomal rupture induced by unmodified mSP1000 was almost completely suppressed by BHA (Fig. 6D). These observations collectively suggest that ROS production induced by phagocytosis of unmodified mSP1000 triggered endosomal rupture followed by the activation of NLRP3 inflammasome and subsequent IL-1 β production. Furthermore, they also strongly indicate that the reduction in ROS production by surface modification attributes to the decrement of the IL-1 β production seen with unmodified mSP1000.

3.7. Cell death by unmodified mSP1000

We reported previously that mSP1000-induced cell death is dependent in part on ROS but independent of caspase-1, -3, -4, and -7, and we also showed that surface modification of mSP1000 significantly suppresses particle cytotoxicity [34]. Here, we speculated that mSP1000-induced cell death was dependent on cathepsin B leakage or on IL-1 β signaling triggered by ROS production. Therefore, to investigate the association of cathepsin B and IL-1 β signaling with mSP1000-induced cell death, we treated THP-1 cells with unmodified mSP1000 in the presence or absence of CA-074-Me, bafilomycin A₁, or zYVAD-fmk. CA-074-Me and bafilomycin A₁, but not zYVAD-fmk, significantly suppressed the cytotoxicity of unmodified mSP1000 (Fig. 6E). These findings indicate that unmodified mSP1000-induced cell death depends in part on ROS and active cathepsin B but is independent of caspases and IL-1 β signals.

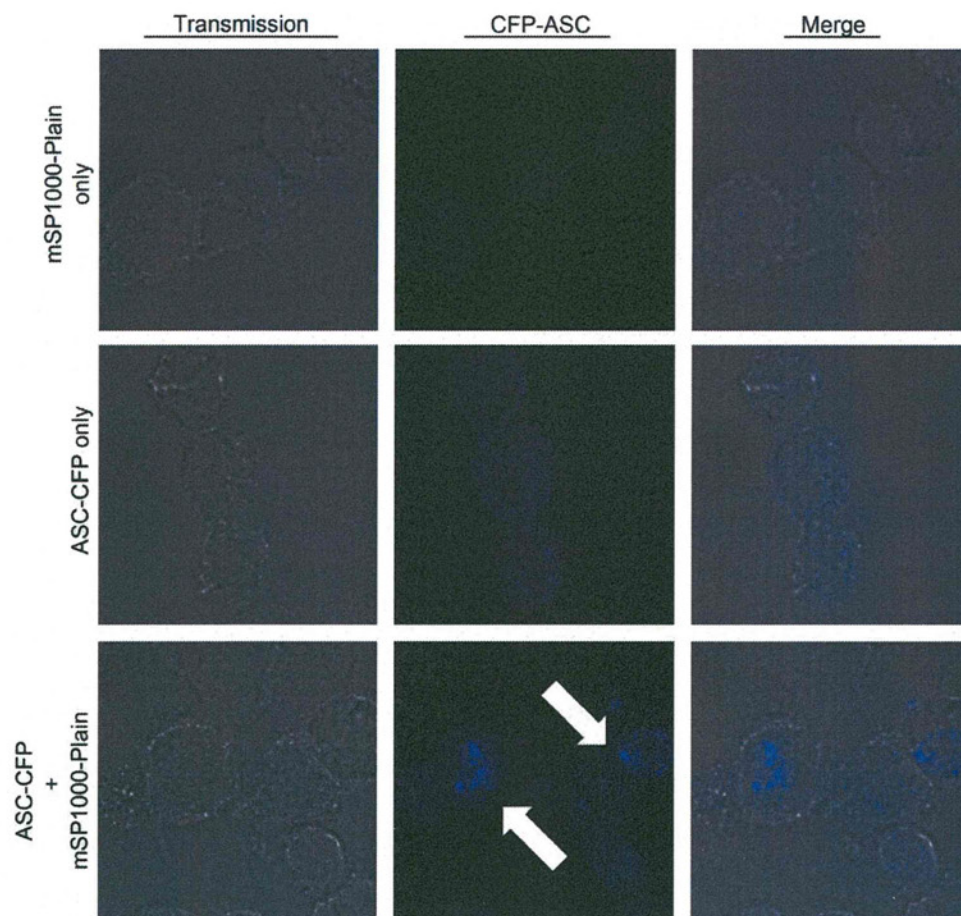


Fig. 4. Unmodified mSP1000-induced IL-1 β production is mediated by activation of NALP3 inflammasome. PMA-primed THP-1 cells transiently transfected with CFP-ASC were treated with unmodified mSP1000. The cells were then observed by confocal microscopy. Treated with unmodified mSP1000 alone (top); untreated but transfected with CFP-ASC (middle); or treated with unmodified mSP1000 and transfected with CFP-ASC (bottom). Arrows indicate clusters of CFP-ASC (blue).

4. Discussion

Our goal was to elucidate the mechanisms of the inflammatory effects induced by SPs and to provide basic information for the creation of safe and effective SPs. To achieve these purposes, we focused on the IL-1 β production induced by SPs, because IL-1 β production is currently considered to play an important role in the initial inflammatory responses that lead to asbestosis and silicosis [19]. Our results provided evidence that unmodified mSP1000, but not smaller SPs, induces significant IL-1 β production by THP-1 cells. Although the detailed mechanisms of this particle-size dependency in IL-1 β production were unclear, we speculate that there are differences in the intracellular behavior of SPs and in the signaling pathways, and cytokine production patterns induced by SPs. Consistent with our hypothesis, our unpublished data showed that mSP1000s and the smaller SPs induce different inflammatory cytokine and chemokine production profiles (data not shown). Furthermore, many reports have shown that nanosized SPs induce inflammation *in vivo*. Therefore, we consider that it is also necessary to investigate the cytokine and chemokine production profiles induced by SPs of various sizes.

We then examined the effects of surface modification on mSP1000-induced IL-1 β production, because it has become evident that surface properties are important factors in the biological effects of particles [14,15]. Interestingly, although unmodified and surface-modified mSP1000s were taken up equally, surface-

modified mSP1000s induce little or no IL-1 β production (Fig. 1B). The *in vivo* inflammatory effect was similarly reduced by surface modification of mSP1000s (Fig. 1C). We consider these results important to the creation of safe SPs.

Next, we examined the mechanisms of IL-1 β production induced by mSP1000s to elucidate why surface modification reduced IL-1 β production. First, we revealed that mSP1000-induced IL-1 β production depends on the activation of NLRP3 inflammasome by using CFP-ASC fusion protein (Fig. 4). Some reports showed that other inflammasomes such as NLRP1 could activate caspase-1 in an ASC-dependent way [35]. Therefore we will need to confirm a specific role for NLRP3 in IL-1 β production induced by mSP1000s by using siRNA of NLRP3 in future. A recent study showed that NLRP3 inflammasome mediated IL-1 β production is associated with fever syndromes characterized by spontaneous inflammation [21]. In fact, the IL-1 β receptor antagonist anakinra has been successfully used to treat patients suffering from inflammatory diseases, indicating that these patients have underlying increased IL-1 β production [36,37]. However, the mechanisms of NLRP3 activation remain unclear, and therefore the definitive target to be overcome for the creation of safe materials is still unknown. Recently, different groups separately reported that cathepsin B leakage after endosomal rupture, as well as cytoplasmic ROS, plays a crucial role in the activation of NLRP3 inflammasome [13,20]. Consistent with these notions, we demonstrated here that mSP1000-induced IL-1 β production is mediated by cathepsin B and

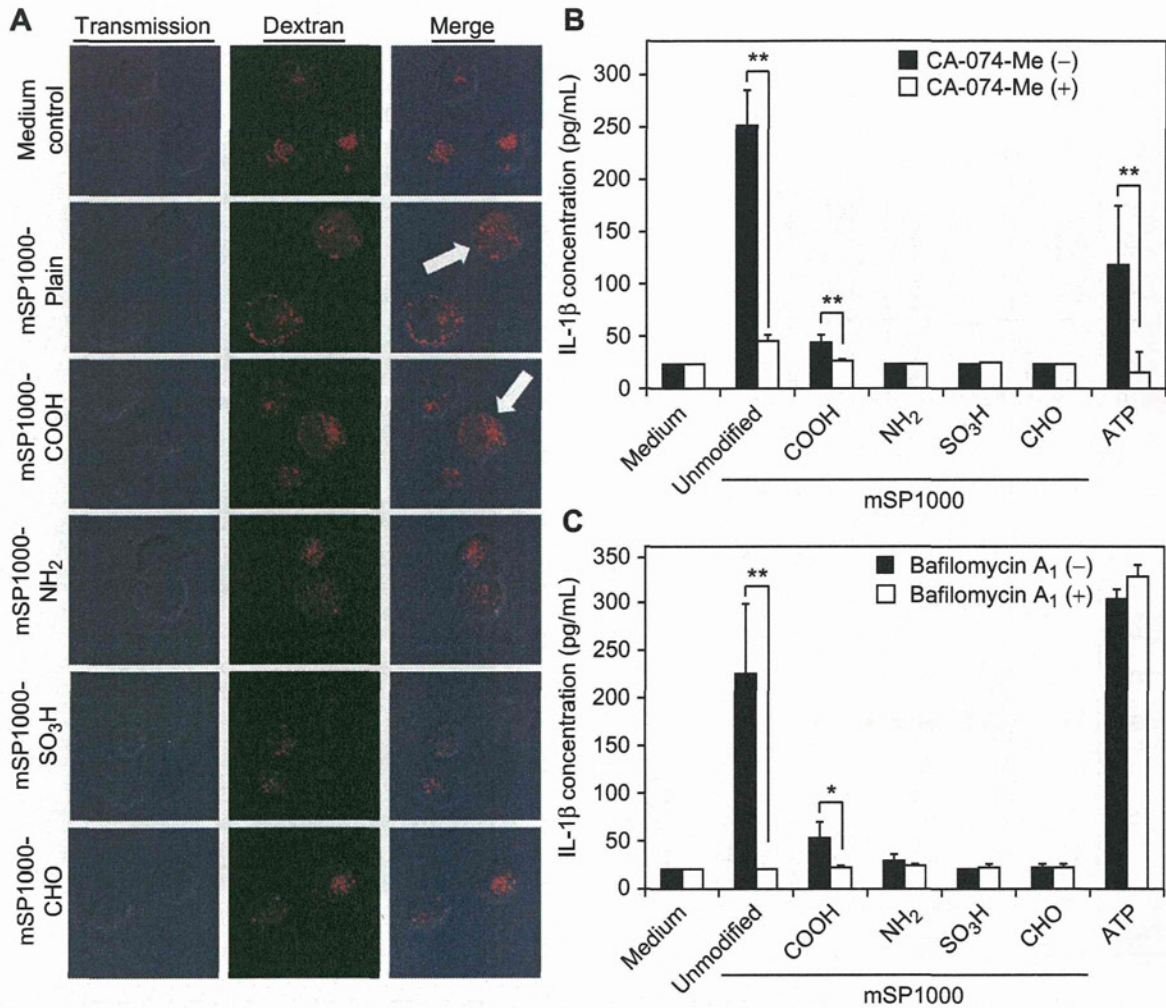


Fig. 5. mSP1000-induced IL-1 β production is mediated by endosomal rupture. (A) Confocal microscopy of endosomal morphology. PMA-primed THP-1 cells were incubated with Alexa Fluor 594-conjugated dextran (red) and each type of mSP1000 for 6 h. The cells were then observed by confocal microscopy. Arrows show cells with spread of dextran into the cytoplasm, indicating endosomal rupture. (B, C) Involvement of cathepsin B in mSP1000-induced IL-1 β production. PMA-primed THP-1 cells were treated with each type of mSP1000 or with ATP for 6 h in the absence (black bars) or presence (white bars) of (B) CA-074-Me (2 μ M) or (C) bafilomycin A₁ (250 nM). Data represent means \pm SD ($n = 5$; * $P < 0.05$, ** $P < 0.01$ versus value for inhibitor [–] control within each treatment pair, t -test).

ROS (Figs. 5 and 6). However, it was unclear whether ROS and cathepsin B activate NLRP3 inflammasome separately or in a coordinated manner, and it was also unclear how endosomal rupture occurred. Use of a ROS inhibitor and surface-modified mSP1000s efficiently suppressed endosomal rupture (Fig. 6D). From these observations, we speculate that, with mSP1000 treatment, ROS trigger endosomal rupture and subsequent cathepsin B leakage into the cytosol, leading to the activation of NLRP3 inflammasome (Fig. 7). Our hypothesis is consistent with some reports suggesting that ROS trigger destabilization of the lysosomal membrane by membrane lipid oxidation [38].

In contrast, some reports have suggested that, in the case of crystalline silica, the reactive particle surface interacts with phagolysosomal membranes, leading to the release of endosomal enzymes into the cytosol after phagocytosis [39–41]. These contradictory findings suggest that various materials induce biological effects by different mechanisms in response to differences in particle characteristics. However, it remains unclear why the surface modification of mSP1000 reduced ROS production. It is possible that inappropriate surface modification induces an

inflammatory effect stronger than that of unmodified SP. We consider that further studies of the relationship between surface characteristics and bio-effect are necessary for the development of safe and effective materials. In this report, we found that DPI, an inhibitor of NADPH oxidase, significantly suppressed mSP1000-induced IL-1 β production (Fig. 6C). NADPH oxidase is activated by the assembly of membrane lipids at local sites on the cellular surface and in the cytoplasm where the particles attach [42,43]. At this point, the silanol group (Si–OH) induces binding of the particles to membranes [44,45]. Therefore, we speculate that surface modification of mSP1000 masks the silanol group from the surface of the mSP1000 and blocks subsequent NADPH oxidase activation.

On the other hand, SP-induced cell death is also a critical obstacle, because macrophages play a central role in host defense systems. In 2007, Willingham et al. proposed a novel cell death pathway called pyronecrosis [46]. Induction of pyronecrosis is not dependent on IL-1 β signaling or caspase-1 activity, although it requires the presence of the inflammasome component ASC and cathepsin B [46–48]. Our data suggested that mSP1000-induced cell death is independent of caspase-1 and IL-1 β signaling but

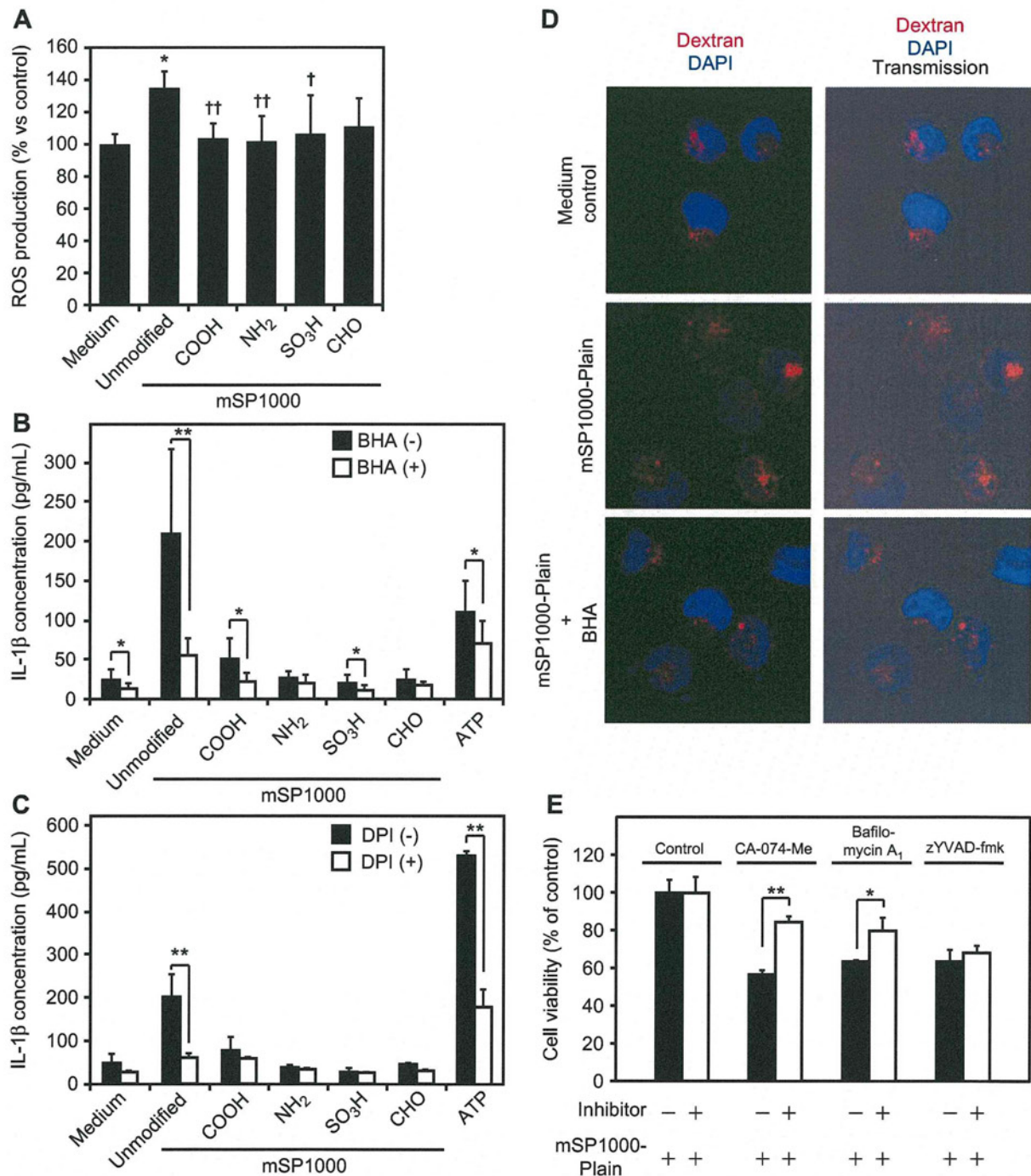


Fig. 6. Unmodified mSP1000-induced ROS production induces endosomal rupture and subsequent IL-1 β production. (A) ROS production levels in PMA-primed THP-1 cells. Cells were treated with each type of mSP1000 for 24 h and incubated with H₂DCFDA (10 μ M) for 45 min. Fluorescence was then measured at OD_{485–530}. ROS production intensity was calculated by the formula ROS production intensity = fluorescence/number of live cells. ROS production intensity of untreated control cells was arbitrarily set to 100%. Data represent means \pm SD ($n = 5$; * $P < 0.05$ versus value for PBS control, [†] $P < 0.05$, ^{††} $P < 0.01$ versus value for unmodified mSP1000, ANOVA). (B, C) Involvement of ROS in mSP1000-induced IL-1 β production. PMA-primed THP-1 cells were treated with each type of mSP1000 or with ATP for 6 h in the absence (black bars) or presence (white bars) of (B) BHA (150 μ M) or (C) DPI (60 μ M), and IL-1 β production levels were measured by ELISA. (D) Confocal microscopy of endosomal morphology. PMA-primed THP-1 cells were incubated with Alexa Fluor 594-conjugated dextran (red) and unmodified mSP1000 for 6 h in the presence (bottom) or absence (middle) of BHA (150 μ M). Cells were then observed by confocal microscopy. Arrows indicate cells with spread of dextran into the cytoplasm. (E) Involvement of cathepsin B and caspase-1 in unmodified mSP1000-induced cytotoxicity. PMA-primed THP-1 cells were treated with unmodified mSP1000 for 24 h in the absence (black bars) or presence (white bars) of CA-074-Me (2 μ M), bafilomycin A₁ (250 nM), or zYVAD-fmk (10 μ M). Cell viability was measured by methylene blue assay. Data represent means \pm SD ($n = 5$; * $P < 0.05$, ** $P < 0.01$ versus value for inhibitor [–] control within each treatment pair, t -test).

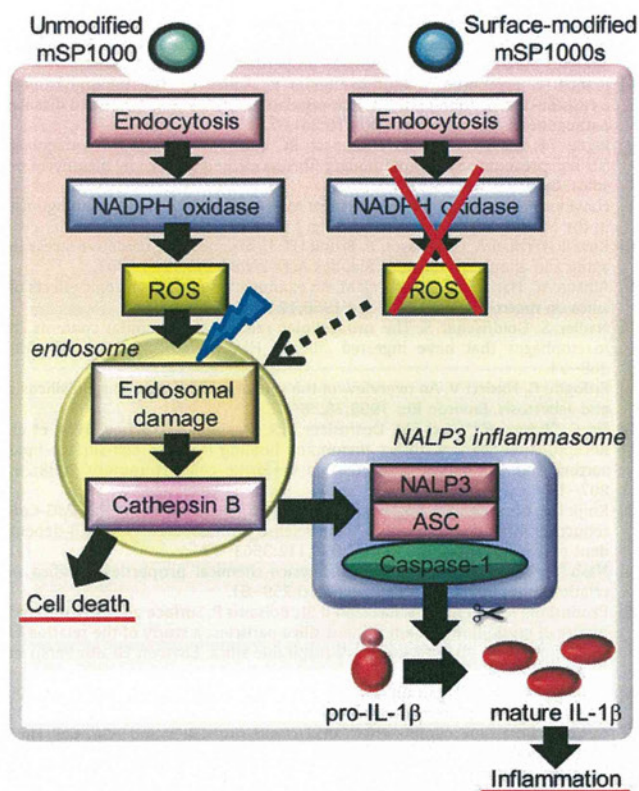


Fig. 7. Model of mSP1000-induced IL-1 β maturation pathways. Unmodified mSP1000-induced IL-1 β maturation is mediated by phagocytosis, activation of NADPH oxidase, ROS production, endosomal rupture, active cathepsin B leakage, assembly of NALP3 inflammasome, and caspase-1 activation. Surface-modified mSP1000s do not activate NADPH oxidase or ROS production, although they are taken up at the same rate as unmodified mSP1000.

dependent on cathepsin B (Fig. 6E) with the ASC assembly (Fig. 4), which means that unmodified mSP1000-induced cell death might occur by pyro necrosis. Pyro necrosis is considered to elicit substantial inflammation and to affect the local environment, whereas apoptosis is widely accepted as non-inflammatory cell death without effects around the dying cells [48]. Thus, pyro necrosis is likely to contribute substantially to the disease state in patients with inflammatory diseases.

We revealed here that SP-induced ROS act as an important upstream signal in the NLRP3 activation pathway. Moreover, we showed that modification of mSP1000s with functional groups suppressed their inflammatory effects. We have since obtained similar results with nanosized particles (nSP70) (unpublished data). These results support our hypothesis that appropriate surface modification of SPs suppresses their inflammatory effect. However, we speculate that blind modification could exacerbate the inflammatory effect, and we consider that an analysis of the mechanisms of the phenomena reported here is necessary.

5. Conclusions

We reveal here that unmodified mSP1000-induced IL-1 β production is mediated by the activation of NADPH oxidase, ROS production, endosomal rupture, active cathepsin B leakage, assembly of NLRP3 inflammasome, and caspase-1 activation. Furthermore, by surface modification with functional groups, we successfully suppressed unmodified mSP1000-induced ROS

production, an upstream signal in the NLRP3 activation pathway, and the subsequent inflammatory responses or cell death. We consider that further studies of the relationship between surface characteristics and biological effects would lead to the development of safe and effective SPs.

Acknowledgements

The authors declare that they have no conflict of interests. We thank Dr. D.T. Golenbock (Department of Infectious Diseases and Immunology, University of Massachusetts Medical School) for providing CFP-ASC plasmid. This study was supported in part by grants from the Ministry of Health, Labor, and Welfare of Japan; by the Ministry of the Environment of Japan; and by the Global COE Program "In Silico Medicine" at Osaka University.

Appendix

Figures with essential color discrimination. Figs. 2, 4–7 in this article are difficult to interpret in black and white. The full color images can be found in the on-line version, at doi:10.1016/j.biomaterials.2010.05.036.

References

- [1] Mossman BT, Churg A. Mechanisms in the pathogenesis of asbestosis and silicosis. *Am J Respir Crit Care Med* 1998;157:1666–80.
- [2] Huaxu F. New developments in the understanding of immunology in silicosis. *Curr Opin Allergy Clin Immunol* 2007;7:168–73.
- [3] Hirsch LR, Stafford RJ, Bankson JA, Sershen SR, Rivera B, Price RE, et al. Nanoshell-mediated near-infrared thermal therapy of tumors under magnetic resonance guidance. *Proc Natl Acad Sci U S A* 2003;100:13549–54.
- [4] Bharali DJ, Klejbor I, Stachowiak EK, Dutta P, Roy I, Kaur N, et al. Organically modified silica nanoparticles: a nonviral vector for in vivo gene delivery and expression in the brain. *Proc Natl Acad Sci U S A* 2005;102:11539–44.
- [5] Roy I, Ohulchanskyy TY, Bharali DJ, Pudavar HE, Mistretta RA, Kaur N, et al. Optical tracking of organically modified silica nanoparticles as DNA carriers: a nonviral, nanomedicine approach for gene delivery. *Proc Natl Acad Sci U S A* 2005;102:279–84.
- [6] Bottini M, D'Annibale F, Magrini A, Cerignoli F, Arimura Y, Dawson MI, et al. Quantum dot-doped silica nanoparticles as probes for targeting of T-lymphocytes. *Int J Nanomedicine* 2007;2:227–33.
- [7] Verraedt E, Pendela M, Adams E, Hoogmartens J, Martens JA. Controlled release of chlorhexidine from amorphous microporous silica. *J Contr Release* 2010;142:47–52.
- [8] Wiethoff AJ, Reed KL, Webb TR, Warheit DB. Assessing the role of neutrophil apoptosis in the resolution of particle-induced pulmonary inflammation. *Inhal Toxicol* 2003;15:1231–46.
- [9] Cho WS, Choi M, Han BS, Cho M, Oh J, Park K, et al. Inflammatory mediators induced by intratracheal instillation of ultrafine amorphous silica particles. *Toxicol Lett* 2007;175:24–33.
- [10] Park EJ, Park K. Oxidative stress and pro-inflammatory responses induced by silica nanoparticles in vivo and in vitro. *Toxicol Lett* 2009;184:18–25.
- [11] Akerman ME, Chan WC, Laakkonen P, Bhatia SN, Ruoslahti E. Nanocrystal targeting in vivo. *Proc Natl Acad Sci U S A* 2002;99:12617–21.
- [12] Kirchner C, Liedl T, Kudera S, Pellegrino T, Munoz Javier A, Gaub HE, et al. Cytotoxicity of colloidal CdSe and CdSe/ZnS nanoparticles. *Nano Lett* 2005;5:331–8.
- [13] Dostert C, Pettrilli V, Van Bruggen R, Steele C, Mossman BT, Tschopp J. Innate immune activation through Nalp3 inflammasome sensing of asbestos and silica. *Science* 2008;320:674–7.
- [14] Albrecht C, Schins RP, Hohl D, Becker A, Shi T, Knaapen AM, et al. Inflammatory time course after quartz instillation: role of tumor necrosis factor- α and particle surface. *Am J Respir Cell Mol Biol* 2004;31:292–301.
- [15] He X, Nie H, Wang K, Tan W, Wu X, Zhang P. In vivo study of biodistribution and urinary excretion of surface-modified silica nanoparticles. *Anal Chem* 2008;80:9597–603.
- [16] Waters KM, Masiello LM, Zangar RC, Tarasevich BJ, Karin NJ, Quesenberry RD, et al. Macrophage responses to silica nanoparticles are highly conserved across particle sizes. *Toxicol Sci* 2009;107:553–69.
- [17] Dinarello CA. Interleukin-1 beta, interleukin-18, and the interleukin-1 beta converting enzyme. *Ann N Y Acad Sci* 1998;856:1–11.
- [18] Pettrilli V, Dostert C, Muruve DA, Tschopp J. The inflammasome: a danger sensing complex triggering innate immunity. *Curr Opin Immunol* 2007;19:615–22.

- [19] Cassel SL, Eisenbarth SC, Iyer SS, Sadler JJ, Colegio OR, Tephly LA, et al. The Nalp3 inflammasome is essential for the development of silicosis. *Proc Natl Acad Sci U S A* 2008;105:9035–40.
- [20] Hornung V, Bauernfeind F, Halle A, Samstad EO, Kono H, Rock KL, et al. Silica crystals and aluminum salts activate the NALP3 inflammasome through phagosomal destabilization. *Nat Immunol* 2008;9:847–56.
- [21] Ting JP, Kastner DL, Hoffman HM. CATERPILLERS, pyrin and hereditary immunological disorders. *Nat Rev Immunol* 2006;6:183–95.
- [22] Martinon F, Petrilli V, Mayor A, Tardivel A, Tschopp J. Gout-associated uric acid crystals activate the NALP3 inflammasome. *Nature* 2006;440:237–41.
- [23] Agostini L, Martinon F, Burns K, McDermott MF, Hawkins PN, Tschopp J. NALP3 forms an IL-1 β -processing inflammasome with increased activity in Muckle-Wells autoinflammatory disorder. *Immunity* 2004;20:319–25.
- [24] Mariathasan S, Weiss DS, Newton K, McBride J, O'Rourke K, Roose-Girma M, et al. Cryopyrin activates the inflammasome in response to toxins and ATP. *Nature* 2006;440:228–32.
- [25] Halle A, Hornung V, Petzold GC, Stewart CR, Monks BG, Reinheckel T, et al. The NALP3 inflammasome is involved in the innate immune response to amyloid- β . *Nat Immunol* 2008;9:857–65.
- [26] Shio MT, Eisenbarth SC, Savaria M, Vinet AF, Bellemare MJ, Harder KW, et al. Malarial hemozoin activates the NLRP3 inflammasome through Lyn and Syk kinases. *PLoS Pathog* 2009;5:e1000559.
- [27] Yoshioka Y, Watanabe H, Morishige T, Yao X, Ikemizu S, Nagao C, et al. Creation of lysine-deficient mutant lymphotoxin- α with receptor selectivity by using a phage display system. *Biomaterials* 2010;31:1935–43.
- [28] Busuttill SJ, Ploplis VA, Castellino FJ, Tang L, Eaton JW, Plow EF. A central role for plasminogen in the inflammatory response to biomaterials. *J Thromb Haemost* 2004;2:1798–805.
- [29] Chung EY, Kim SJ, Ma XJ. Regulation of cytokine production during phagocytosis of apoptotic cells. *Cell Res* 2006;16:154–61.
- [30] Fernandes-Alnemri T, Wu J, Yu JW, Datta P, Miller B, Jankowski W, et al. The pyroptosome: a supramolecular assembly of ASC dimers mediating inflammatory cell death via caspase-1 activation. *Cell Death Differ* 2007;14:1590–604.
- [31] Magalhaes AC, Baron GS, Lee KS, Steele-Mortimer O, Dorward D, Prado MA, et al. Uptake and neuritic transport of scrapie prion protein coincident with infection of neuronal cells. *J Neurosci* 2005;25:5207–16.
- [32] Egler RA, Fernandes E, Rothermund K, Sereika S, de Souza-Pinto N, Jaruga P, et al. Regulation of reactive oxygen species, DNA damage, and c-Myc function by peroxiredoxin 1. *Oncogene* 2005;24:8038–50.
- [33] Morel F, Doussiere J, Vignais PV. The superoxide-generating oxidase of phagocytic cells. Physiological, molecular and pathological aspects. *Eur J Biochem* 1991;201:523–46.
- [34] Morishige A, Yoshioka Y, Inakura H, Tanabe A, Yao X, Tsunoda SI, et al. Cytotoxicity of amorphous silica particles against macrophage-like THP-1 cells depends on particle-size and surface properties. *Pharmazie* in press.
- [35] Franchi L, Eigenbrod T, Munoz-Planillo R, Nunez G. The inflammasome: a caspase-1-activation platform that regulates immune responses and disease pathogenesis. *Nat Immunol* 2009;10:241–7.
- [36] Piguet PF, Vesin C, Grau GE, Thompson RC. Interleukin 1 receptor antagonist (IL-1ra) prevents or cures pulmonary fibrosis elicited in mice by bleomycin or silica. *Cytokine* 1993;5:57–61.
- [37] Hawkins PN, Lachmann HJ, McDermott MF. Interleukin-1-receptor antagonist in the Muckle-Wells syndrome. *N Engl J Med* 2003;348:2583–4.
- [38] Kurz T, Terman A, Gustafsson B, Brunk UT. Lysosomes and oxidative stress in aging and apoptosis. *Biochim Biophys Acta* 2008;1780:1291–303.
- [39] Allison AC, Harington JS, Birbeck M. An examination of the cytotoxic effects of silica on macrophages. *J Exp Med* 1966;124:141–54.
- [40] Nadler S, Goldfischer S. The intracellular release of lysosomal contents in macrophages that have ingested silica. *J Histochem Cytochem* 1970;18:368–71.
- [41] Erdogdu G, Hasirci V. An overview of the role of mineral solubility in silicosis and asbestosis. *Environ Res* 1998;78:38–42.
- [42] Ng G, Sharma K, Ward SM, Desrosiers MD, Stephens LA, Schoel WM, et al. Receptor-independent, direct membrane binding leads to cell-surface lipid sorting and Syk kinase activation in dendritic cells. *Immunity* 2008;29:807–18.
- [43] Kuijk LM, Beekman JM, Koster J, Waterham HR, Frenkel J, Coffey PJ. HMG-CoA reductase inhibition induces IL-1 β release through Rac1/PI3K/PKB-dependent caspase-1 activation. *Blood* 2008;112:3563–73.
- [44] Nash T, Allison AC, Harington JS. Physico-chemical properties of silica in relation to its toxicity. *Nature* 1966;210:259–61.
- [45] Pandurangi RS, Seehra MS, Razzaboni BL, Bolsaitis P. Surface and bulk infrared modes of crystalline and amorphous silica particles: a study of the relation of surface structure to cytotoxicity of respirable silica. *Environ Health Perspect* 1990;86:327–36.
- [46] Willingham SB, Bergstralh DT, O'Connor W, Morrison AC, Taxman DJ, Duncan JA, et al. Microbial pathogen-induced necrotic cell death mediated by the inflammasome components CIAS1/cryopyrin/NLRP3 and ASC. *Cell Host Microbe* 2007;2:147–59.
- [47] Fujisawa A, Kambe N, Saito M, Nishikomori R, Tanizaki H, Kanazawa N, et al. Disease-associated mutations in CIAS1 induce cathepsin B-dependent rapid cell death of human THP-1 monocytic cells. *Blood* 2007;109:2903–11.
- [48] Ting JP, Willingham SB, Bergstralh DT. NLRs at the intersection of cell death and immunity. *Nat Rev Immunol* 2008;8:372–9.

Laboratory of Biotechnology and Therapeutics¹, Graduate School of Pharmaceutical Sciences; The Center for Advanced Medical Engineering and Informatics², Osaka University; Laboratory of Pharmaceutical Proteomics³, National Institute of Biomedical Innovation, Laboratory of Toxicology and Safety Science⁴, Graduate School of Pharmaceutical Sciences, Osaka University, Osaka, Japan

Cytotoxicity of amorphous silica particles against macrophage-like THP-1 cells depends on particle-size and surface properties

T. MORISHIGE^{1,*}, Y. YOSHIOKA^{1,2,*}, H. INAKURA¹, A. TANABE¹, X. YAO¹, S. TSUNODA^{2,3}, Y. TSUTSUMI^{2,3,4}, Y. MUKAI¹, N. OKADA¹, S. NAKAGAWA^{1,2}

Received December 17, 2009, accepted January 4, 2010

Yasuo Yoshioka, Ph.D., The Center for Advanced Medical Engineering and Informatics, Osaka University, 1-6 Yamadaoka, Suita, Osaka 565-0871, Japan

yasuo@phs.osaka-u.ac.jp

* Each author contributed equally to the work.

Pharmazie 65: 1–4 (2010)

doi: 10.1691/ph.2010.9408

Recent studies have indicated that amorphous silica particles (SPs) show cytotoxicity against various types of cells, including macrophages. However, the mechanism of cell death has not been determined, and systematic investigations of the relationship between particle characteristics and cytotoxicity are still quite limited. Here, we compared the cytotoxicity of SPs of various sizes (30–1000 nm) and surface properties against differentiated THP-1 human macrophage-like cells. We found that 300 and 1000 nm SPs showed cytotoxicity against THP-1 cells, whereas 30, 50, and 70 nm SPs did not induce cell death. We demonstrated that 1000 nm SP showed strong cytotoxicity that depended on reactive oxygen species but was independent of caspases. Furthermore, we showed that surface modification of 1000 nm SPs dramatically suppressed their cytotoxicity. Our results suggest that systematic evaluation of the association between particle characteristics and biological effects is necessary for the creation of safe SPs.

1. Introduction

Amorphous (noncrystalline) silica particles (SPs) possess useful properties, including straightforward synthesis, relatively low cost, easy separation, high hydrophilicity, and facile surface modification. In addition, SPs are usually considered to have low toxicity, in contrast to crystalline silica, which can cause silicosis and some forms of lung cancer (Mossman and Churg 1998; Huaux 2007). Therefore, SPs have been used for many applications, including cosmetics, foods, medical diagnosis, cancer therapy, and drug delivery (Hirsch et al. 2003; Bharali et al. 2005; Roy et al. 2005; Bottini et al. 2007; Verraedt et al. 2009).

However, the increasing use of SPs has raised public concern about their safety. In fact, recent studies have found that SPs induce substantial lung inflammation and are cytotoxic against various cells, including macrophages (Wiethoff et al. 2003; Cho et al. 2007; Napierska et al. 2009). Thus, the safety and overall biological effects of SPs have been questioned (Akerman et al. 2002; Kirchner et al. 2005; Dostert et al. 2008). In addition, it has recently become evident that particle characteristics, including particle size and surface properties, are important factors in pathologic alterations and cellular responses (Albrecht et al. 2004; He et al. 2008; Waters et al. 2009). Therefore, investigation of the mechanisms of SP-induced inflammation and cytotoxicity and of the relationship between particle characteristics and cytotoxicity is important for the development of safe SPs.

Here we demonstrate that SPs exhibit cytotoxicity against THP-1 human macrophage-like cells in a size-dependent man-

Pharmazie 65 (2010)

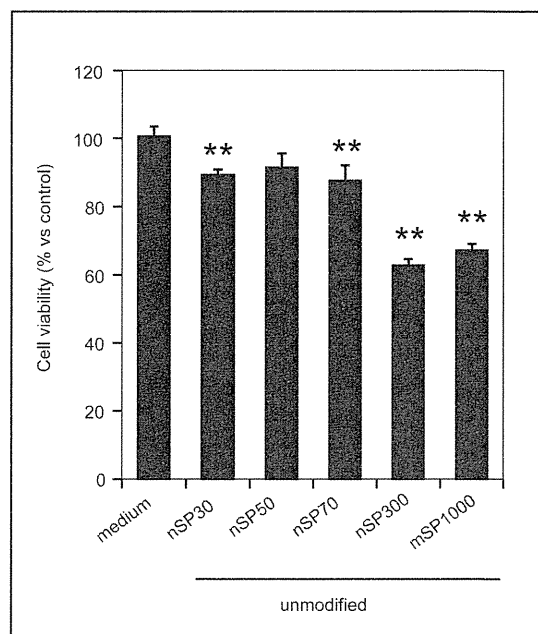


Fig. 1: Correlation between SP particle size and cytotoxicity against macrophage-like cells. PMA-primed THP-1 cells were treated with 100 μ g/mL unmodified SPs for 24 h, and cell viability was evaluated by means of the standard methylene blue assay. The data represent the mean \pm SD ($n=5$; ** $P < 0.01$ versus value for medium control)

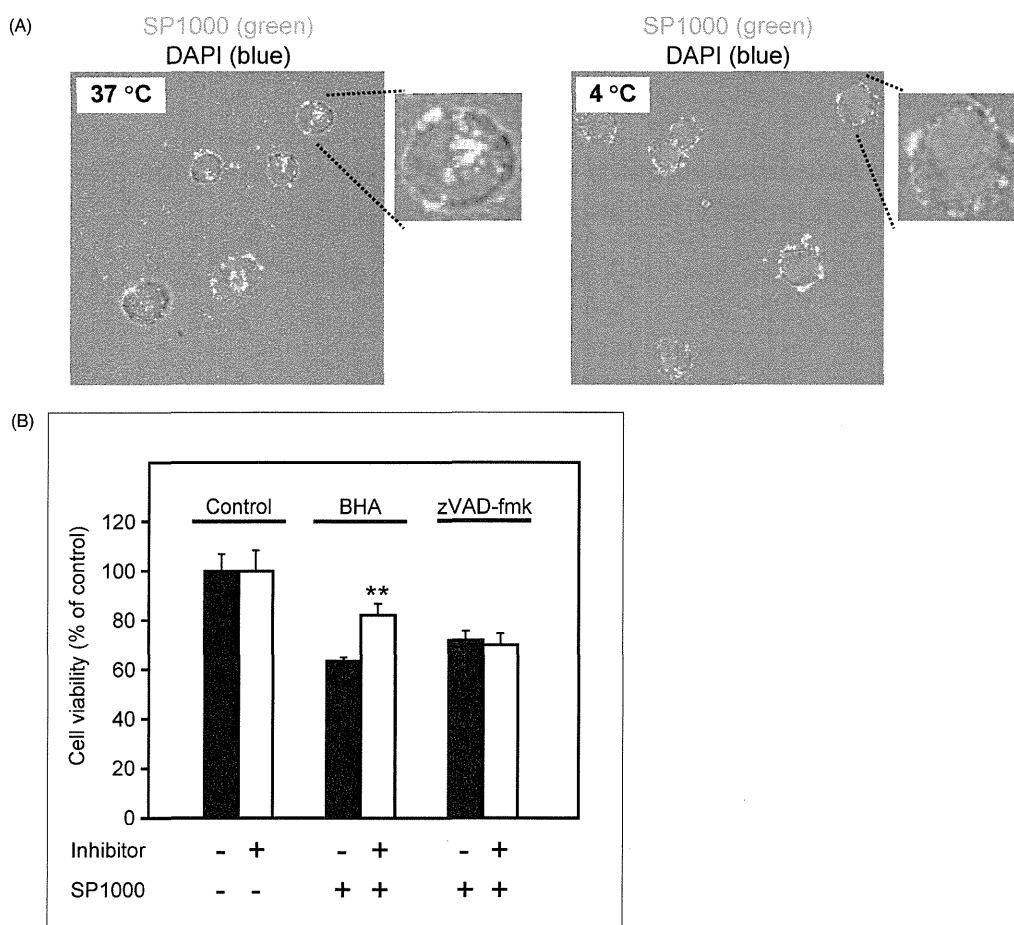


Fig. 2: ROS and caspase dependence of mSP1000-induced cell death. (A) Confocal microscopy images of the ingestion of mSP1000. FITC-conjugated mSP1000 (green) were added to the PMA-primed THP-1 cells at 100 µg/mL. Cells were incubated for 6 h at 37 °C (left) or 4 °C (right). The nucleus was stained with DAPI (blue). (B) Effect of a caspase inhibitor and an ROS scavenger on cytotoxicity of mSP1000. PMA-primed THP-1 cells were treated with 100 µg/mL SP1000s for 24 h in the presence or absence of BHA (150 µM) or zVAD-fmk (60 µM). Cell viability was measured by means of the methylene blue assay. The data represent the mean ± SD (n = 4; **P < 0.01 versus value for inhibitor [-] control)

ner. Furthermore, we show that SPs with diameters of 1000 nm induce the production of reactive oxygen species (ROS), which triggers THP-1 cell death. We also demonstrate that surface modification of SPs with various functional groups significantly suppresses SP cytotoxicity.

2. Investigations, results and discussion

In this study, we examined whether the size and surface characteristics of SPs are correlated with their cytotoxicity. We also investigated the mechanism by which SPs induce the death of macrophage-like THP-1 cells, with the goal of providing information for the creation of novel safe SPs.

2.1. Amorphous silica particles induce cell death in a size-dependent manner

We used five SPs with diameters between 30 and 1000 nm (nSP30, nSP50, nSP70, nSP300, and mSP1000); the mean secondary particle diameters of the SPs measured by means of a Zetasizer were 33, 44, 79, 326, and 945 nm, respectively

(data not shown). To compare the cytotoxicities of the SPs with different diameters, we examined their cytotoxicity against macrophages, which are the first line of defense against infection or injury from various inhaled agents. We incubated phorbol 12-myristate 13-acetate (PMA)-primed human macrophage-like THP-1 cells with SPs and analyzed the levels of cell viability. Twenty-four hours after the incubation, we found that nSP300 and mSP1000 induced marked cytotoxicity, whereas nSP30, nSP50, and nSP70 showed no cytotoxicity (Fig. 1). These results indicate that the particle size of the SPs was intimately involved in their biological effects.

2.2. mSP1000-induced cytotoxicity depends on ROS but not on caspases

Macrophages remove inhaled agents including foreign particles by means of their phagocytic activity. To confirm that THP-1 cells took up mSP1000, we treated THP-1 cells with fluorescein-5-isothiocyanate (FITC)-conjugated mSP1000 at 37 °C or 4 °C. We visually confirmed that mSP1000 were ingested into THP-1 cells at 37 °C, whereas only adsorption of mSP1000 on the cellular surface was detected at 4 °C (Fig. 2A). These results

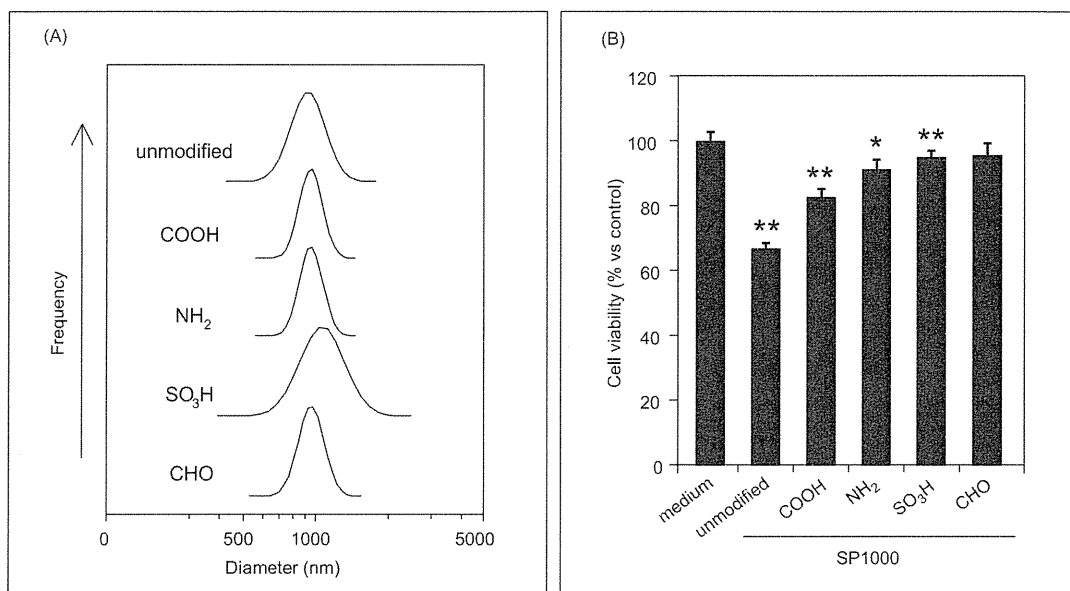


Fig. 3: Correlation between surface modification of mSP1000s and cytotoxicity against macrophage-like THP-1 cells. (A) Particle size distributions of unmodified and surface-modified mSP1000s. Particle size distributions were measured with a Zetasizer 3000HS after sonication at a particle concentration of 300 (g/mL in H₂O). (B) Cytotoxicity of surface-modified mSP1000s. PMA-primed THP-1 cells were treated with the surface-modified mSP1000s at 100 µg/mL for 24 h. After the stimulation, cell viability was measured by means of the standard methylene blue assay. The data represent the mean ± SD ($n=5$; ** $P < 0.01$, * $P < 0.05$ versus value for medium control)

indicate that mSP1000 were recognized and taken up into THP-1 cells by energy-dependent phagocytosis.

We next examined the mechanism of mSP1000-induced cytotoxicity. To determine whether there was an association between caspases and mSP1000-induced cell death, we treated cells with mSP1000 in the presence or absence of zVAD-fmk, a broad caspase inhibitor (it inhibits caspase-1, -3, -4, and -7). We found that zVAD-fmk did not affect the mSP1000-induced cytotoxicity, which indicates that the cytotoxicity was independent of caspases (Fig. 2B). Recently, four kinds of cell death pathways were reported: apoptosis, necrosis, pyroptosis, and pyronecrosis (Ting et al. 2008). Apoptosis and pyroptosis are dependent on the activity of caspases, whereas necrosis and pyronecrosis are independent of caspases. Therefore, our results suggest that mSP1000-induced cell death might have been necrosis or pyronecrosis. Both pathways elicit substantial inflammation, whereas apoptosis is a non-inflammatory cell death that does not affect the area around the dying cells (Ting et al. 2008). Therefore, we suspected that SP-induced cell death might be associated with inflammatory responses induced by mSP1000. However, the stimulation of macrophages with materials such as silica is known to induce ROS production (Msiska et al. 2009). Excessive production of ROS itself causes irreversible cellular injuries and contributes to the pathogenesis of several inflammatory diseases (Cross et al. 1994; Terman et al. 2006). To determine whether ROS were involved in mSP1000-induced cell death, we stimulated THP-1 cells with mSP1000 in the presence of a broad ROS scavenger, butylated hydroxyanisole (BHA), and found that the scavenger significantly inhibited the cytotoxicity of mSP1000 (Fig. 2B). These results indicate that ROS played an important role in the mSP1000-induced cell death and that the cytotoxicity induced by mSP1000 depends on ROS production but is independent of caspases, which suggests that mSP1000-induced cell death is inflammatory necrosis or pyronecrosis.

Pharmazie 65 (2010)

2.3. mSP1000-induced cell death is suppressed by surface modification with functional groups

To assess the correlation between surface modification and SP cytotoxicity, we used mSP1000 modified with various surface functional groups (-COOH, -NH₂, -SO₃H, and -CHO). The mean secondary particle diameters of unmodified mSP1000 was 945 nm, and the corresponding values for the modified particles were 1022, 958, 1023, and 969 nm, respectively (Fig. 3A). We compared the cytotoxicity of the modified and unmodified particles against THP-1 cells and found that mSP1000-induced cytotoxicity was suppressed by the surface modification (Fig. 3B). Interestingly, we confirmed that all the surface-modified mSP1000 were taken up equally into the cells (data not shown). We expect that surface modification can be used as a novel method to create safe SPs.

In summary, we confirmed that the cytotoxicity of SPs depended on particle size and surface properties. We confirmed that mSP1000-induced cell death was dependent on ROS production but independent of caspases. We believe that this information will be useful for the creation of novel safe SP-based materials.

3. Experimental

3.1. Materials and reagents

We used SPs with diameters between 30 and 1000 nm (nSP30, nSP50, nSP70, nSP300, and mSP1000), and mSP1000s with various surface functional groups (-COOH, -NH₂, -SO₃H, and -CHO). The SPs (Sicaster) were purchased from Micromod Partikeltechnologie (Rostock/Warnemünde, Germany). PMA and BHA were purchased from Sigma (St. Louis, MO). zVAD-fmk was purchased from Merck Calbiochem (Darmstadt, Germany).

3.2. Cell treatment

THP-1 cells (human acute monocytic leukemia cell line) were obtained from the American Type Culture Collection (Manassas, VA) and were cultured in RPMI-1640 (Wako Pure Chemical Industries, Osaka, Japan) supplemented

with 10% fetal bovine serum, 2 mM L-glutamine, and antibiotics at 37 °C. Treatment of THP-1 cells with PMA reportedly induces differentiation to a macrophage phenotype (Hoff et al. 1992; Rutault et al. 2001).

3.3. Size distribution of silica particles

The size distributions of the SP were measured with a Zetasizer 3000HS (Malvern, Worcestershire, UK) after sonication at a particle concentration of 300 µg/mL in H₂O.

3.4. Cytotoxicity of various silica particles

THP-1 cells (1.5 × 10⁴ cells/well) were seeded in 96-well plates, differentiated to macrophages by incubation with 0.5 µM PMA for 24 h, and then washed once with incubation medium. After the PMA priming, cells were treated with 100 µg/mL SPs for 24 h. The cytotoxicity of the SPs against THP-1 cells was assessed by means of the standard methylene blue assay. In brief, after the SP treatment, cells were fixed with 100 µL of 2.5% glutaraldehyde for 15 min and stained with 100 µL of 0.05% methylene blue for 15 min. Then, the cells were lysed with 200 µL of 0.33 N HCl. The OD_{655–415} was measured using a multiwell spectrophotometer (Molecular Devices, Inc., Tokyo, Japan).

For the inhibitory assays, PMA-primed THP-1 cells were pre-incubated with BHA (150 µM) or zVAD-fmk (60 µM) for 30 min and then treated with 100 µg/mL SPs for 24 h in the presence or absence of each inhibitor.

3.5. Laser scanning confocal microscopy analysis

THP-1 cells (1.0 × 10⁵ cells/well) were seeded on Lab-Tek II Chambered Coverglass (Nunc, Rochester, NY), differentiated to macrophages by incubation with 0.5 µM PMA for 24 h, and treated for 6 h with 100 µg/mL mSP1000s. Then the cells were washed and fixed with 4% paraformaldehyde and mounted with Prolong Gold with 2-(4-amidinophenyl)-1H-indole-6-carboxamide (DAPI, Invitrogen, Carlsbad, CA) for nuclear staining. Fluorescence was observed with a laser scanning confocal microscope (Leica Microsystems GmbH, Wetzlar, Germany).

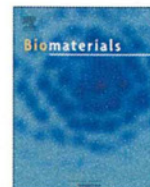
3.6. Statistical analysis

All results are presented as means ± standard deviation (SD). Differences were compared using Student's *t*-test or Scheffé's method after analysis of variance (ANOVA).

Acknowledgements: The authors declare that they have no conflicts of interest. This study was supported in part by grants from the Ministry of Health, Labor, and Welfare in Japan.

References

- Akerman ME, Chan WC, Laakkonen P, Bhatia SN, Ruoslahti E (2002) Nanocrystal targeting *in vivo*. *Proc Natl Acad Sci U S A* 99: 12617–12621.
- Albrecht C, Schins RP, Hohl D, Becker A, Shi T, Knaepen AM, Borm PJ (2004) Inflammatory time course after quartz instillation: role of tumor necrosis factor- α and particle surface. *Am J Respir Cell Mol Biol* 31: 292–301.
- Bharali DJ, Klejbor I, Stachowiak EK, Dutta P, Roy I, Kaur N, Bergey EJ, Prasad PN, Stachowiak MK (2005) Organically modified silica nanoparticles: a nonviral vector for *in vivo* gene delivery and expression in the brain. *Proc Natl Acad Sci U S A* 102: 11539–11544.
- Bottini M, D'Annibale F, Magrini A, Cerignoli F, Arimura Y, Dawson MI, Bergamaschi E, Rosato N, Bergamaschi A, Mustelin T (2007) Quantum dot-doped silica nanoparticles as probes for targeting of T-lymphocytes. *Int J Nanomedicine* 2: 227–233.
- Cho WS, Choi M, Han BS, Cho M, Oh J, Park K, Kim SJ, Kim SH, Jeong J (2007) Inflammatory mediators induced by intratracheal instillation of ultrafine amorphous silica particles. *Toxicol Lett* 175: 24–33.
- Cross CE, van der Vliet A, O'Neill CA, Eiserich JP (1994) Reactive oxygen species and the lung. *Lancet* 344: 930–933.
- Dostert C, Petrilli V, Van Bruggen R, Steele C, Mossman BT, Tschopp J (2008) Innate immune activation through Nalp3 inflammasome sensing of asbestos and silica. *Science* 320: 674–677.
- He X, Nie H, Wang K, Tan W, Wu X, Zhang P (2008) *In vivo* study of biodistribution and urinary excretion of surface-modified silica nanoparticles. *Anal Chem* 80: 9597–9603.
- Hirsch LR, Stafford RJ, Bankson JA, Sershen SR, Rivera B, Price RE, Hazle JD, Halas NJ, West JL (2003) Nanoshell-mediated near-infrared thermal therapy of tumors under magnetic resonance guidance. *Proc Natl Acad Sci U S A* 100: 13549–13554.
- Hoff T, Spencker T, Emmendoerffer A, Goppelt-Strube M (1992) Effects of glucocorticoids on the TPA-induced monocytic differentiation. *J Leukoc Biol* 52: 173–182.
- Huax F (2007) New developments in the understanding of immunology in silicosis. *Curr Opin Allergy Clin Immunol* 7: 168–173.
- Kirchner C, Liedl T, Kudera S, Pellegrino T, Munoz Javier A, Gaub HE, Stolzle S, Fertig N, Parak WJ (2005) Cytotoxicity of colloidal CdSe and CdSe/ZnS nanoparticles. *Nano Lett* 5: 331–338.
- Mossman BT, Churg A (1998) Mechanisms in the pathogenesis of asbestosis and silicosis. *Am J Respir Crit Care Med* 157: 1666–1680.
- Msiska Z, Pacurari M, Mishra A, Leonard SS, Castranova V, Vallyathan V (2009) DNA double strand breaks by asbestos, silica and titanium dioxide: possible biomarker of carcinogenic potential? *Am J Respir Cell Mol Biol* in print.
- Napierska D, Thomassen LC, Rabolli V, Lison D, Gonzalez L, Kirsch-Volders M, Martens JA, Hoet PH (2009) Size-dependent cytotoxicity of monodisperse silica nanoparticles in human endothelial cells. *Small* 5: 846–853.
- Roy I, Ohulchanskyy TY, Bharali DJ, Pudavar HE, Mistretta RA, Kaur N, Prasad PN (2005) Optical tracking of organically modified silica nanoparticles as DNA carriers: a nonviral, nanomedicine approach for gene delivery. *Proc Natl Acad Sci U S A* 102: 279–284.
- Rutault K, Hazzalin CA, Mahadevan LC (2001) Combinations of ERK and p38 MAPK inhibitors ablate tumor necrosis factor- α (TNF- α) mRNA induction. Evidence for selective destabilization of TNF- α transcripts. *J Biol Chem* 276: 6666–6674.
- Terman A, Gustafsson B, Brunk UT (2006) The lysosomal-mitochondrial axis theory of postmitotic aging and cell death. *Chem Biol Interact* 163: 29–37.
- Ting JP, Willingham SB, Bergstralh DT (2008) NLRs at the intersection of cell death and immunity. *Nat Rev Immunol* 8: 372–379.
- Verraedt E, Pendela M, Adams E, Hoogmartens J, Martens JA (2009) Controlled release of chlorhexidine from amorphous microporous silica. *J Control Release*.
- Waters KM, Masiello LM, Zangar RC, Tarasevich BJ, Karin NJ, Quesenberry RD, Bandyopadhyay S, Teeguarden JG, Pounds JG, Thrall BD (2009) Macrophage responses to silica nanoparticles are highly conserved across particle sizes. *Toxicol Sci* 107: 553–569.
- Wiethoff AJ, Reed KL, Webb TR, Warheit DB (2003) Assessing the role of neutrophil apoptosis in the resolution of particle-induced pulmonary inflammation. *Inhal Toxicol* 15: 1231–1246.



Leading Opinion

Acute phase proteins as biomarkers for predicting the exposure and toxicity of nanomaterials[☆]

Kazuma Higashisaka^{a,b,1}, Yasuo Yoshioka^{a,b,c,*,1}, Kohei Yamashita^{a,b}, Yuki Morishita^{a,b}, Maho Fujimura^{a,b}, Hiromi Nabeshi^a, Kazuya Nagano^b, Yasuhiro Abe^b, Haruhiko Kamada^{b,c}, Shin-ichi Tsunoda^{b,c,d}, Tomoaki Yoshikawa^{a,b}, Norio Itoh^a, Yasuo Tsutsumi^{a,b,c,**}

^a Department of Toxicology and Safety Science, Graduate School of Pharmaceutical Sciences, Osaka University, 1-6 Yamadaoka, Suita, Osaka 565-0871, Japan

^b Laboratory of Pharmaceutical Proteomics, National Institute of Biomedical Innovation, 7-6-8, Saito-Asagi, Ibaraki, Osaka 567-0085, Japan

^c The Center for Advanced Medical Engineering and Informatics, Osaka University, 1-6, Yamadaoka, Suita, Osaka 565-0871, Japan

^d Department of Biomedical Innovation, Graduate School of Pharmaceutical Sciences, Osaka University, 7-6-8, Saito-Asagi, Ibaraki, Osaka 567-0085, Japan

ARTICLE INFO

Article history:

Received 8 July 2010

Accepted 31 August 2010

Available online 22 September 2010

Keywords:

Nanoparticle

Plasma proteins

Silica

Surface modification

ABSTRACT

Recently, nanomaterials have become an integral part of our daily lives. However, there is increasing concern about the potential risk to human health. Here, we attempted to identify biomarkers for predicting the exposure and toxicity of nanomaterials by using a proteomics based approach. We evaluated the changes of protein expression in plasma after treatment with silica nanoparticles. Our analyses identified haptoglobin, one of the acute phase proteins, as a candidate biomarker. The results of ELISA showed that the level of haptoglobin was significantly elevated in plasma of mice exposed to silica nanoparticles with a diameter of 70 nm (nSP70) compared to normal mice and those exposed to silica particles with a diameter of 1000 nm. Furthermore, the other acute phase proteins, C-reactive protein (CRP) and serum amyloid A (SAA) were also elevated in plasma of nSP70 treated mice. In addition, the level of these acute phase proteins was elevated in the plasma of mice after intranasal treatment with nSP30. Our results suggest that haptoglobin, CRP and SAA are highly sensitive biomarkers for assessing the risk of exposure to silica nanoparticles. We believe this study will contribute to the development of global risk assessment techniques for nanomaterials.

© 2010 Elsevier Ltd. All rights reserved.

1. Introduction

With the recent development of nanotechnology, nanomaterials such as silica nanoparticles are beginning to be used on a global scale. In comparison to conventional materials with submicron size, nanomaterials display unique properties such as high levels of

electrical conductivity, tensile strength and chemical reactivity [1]. Nanomaterials have already been used in various fields such as electronic engineering, cosmetics and medicine [2,3]. Because nanotechnology is emerging as a leading industrial sector, humans will be increasingly exposed to a wide range of synthetic nanomaterials with diverse properties.

The increasing use of nanomaterials has raised public concerns about the potential risks to human health [4–6]. For example, it is reported that carbon nanotubes induce mesothelioma-like lesions in mice in a similar way to crocidolite asbestos [7]. Other reports showed that exposure to titanium dioxide particles induce inflammatory responses and lung injury in mice [8,9]. In addition, our group showed that silica nanoparticles with a diameter of 70 nm can penetrate mouse skin and enter the circulatory system (unpublished data). Furthermore our group demonstrated that silica nanoparticles induce severe liver damage after systemic administration [10–12]. However, current knowledge of the potential risk of nanomaterials is considered insufficient. Indeed, concerns about the potential dangers of nanomaterials have led the World Health Organization and the Organization for Economic

[☆] *Editor's Note:* This paper is one of a newly instituted series of scientific articles that provide evidence-based scientific opinions on topical and important issues in biomaterials science. They have some features of an invited editorial but are based on scientific facts, and some features of a review paper, without attempting to be comprehensive. These papers have been commissioned by the Editor-in-Chief and reviewed for factual, scientific content by referees.

* Corresponding author. The Center for Advanced Medical Engineering and Informatics, Osaka University, 1-6 Yamadaoka, Suita, Osaka 565-0871, Japan. Tel.: +81 6 6879 8230; fax: +81 6 6879 8234.

** Corresponding author. Department of Toxicology and Safety Science, Graduate School of Pharmaceutical Sciences, Osaka University, 1-6, Yamadaoka, Suita, Osaka 565-0871, Japan. Tel.: +81 6 6879 8230; fax: +81 6 6879 8234.

E-mail addresses: yasuo@phs.osaka-u.ac.jp (Y. Yoshioka), ytsutsumi@phs.osaka-u.ac.jp (Y. Tsutsumi).

¹ These authors contributed equally to the work.

Co-operation and Development to call for an urgent and detailed evaluation of their safety. Therefore, it is extremely important to progress these safety evaluations in order to facilitate the development of nanomaterials that are harmless to humans, because nanomaterials have the potential to improve the quality of human life. In particular, it is hoped that a risk assessment system can be developed to estimate or predict the safety and toxicity of nanomaterials.

Molecular biomarkers, obtained from biological samples such as blood, urine and tissue, constitute an objective indicator for correlating against various physiological conditions or variation of disease state [13,14]. By using biomarkers, we are able to predict not only the present disease and clinical condition but the risk of acquiring disease in the future. Nowadays, biomarkers that act as predictors of cancer have already been developed and are commonly used in clinical practice [14]. Furthermore, such an approach is capable of predicting adverse effects of drugs and medicines [15,16]. By contrast, studies of biomarkers for nanomaterials have barely advanced. These biomarkers would represent the unity of local and systemic physiological responses induced as a result of the exposure. Therefore, biomarkers for nanomaterials will be invaluable for predicting their potential toxicity and establishing strategies for the safe development of nanomaterials production and use.

Here we attempted to develop potential biomarkers of nanomaterials using a proteomics analysis with the aim of developing safe forms of nanomaterials.

2. Materials and methods

2.1. Materials

Silica particles were purchased from Micromod Partikeltechnologie (Rostock/Warnemünde, Germany). The silica particles with diameters of 30, 70, 300 and 1000 nm (nSP30, nSP70, nSP300 and mSP1000, respectively), and nSP70 with surface functional groups such as carboxyl group and amino group (nSP70-C and nSP70-N, respectively) were used in this study. The silica particles were sonicated for 5 min and vortexed for 1 min prior to use.

2.2. Animals

Female BALB/c mice were purchased from Nippon SLC, Inc (Shizuoka, Japan) and used at 6–8 weeks of age. All of the animal experimental procedures in this study were performed in accordance with the National Institute of Biomedical Innovation guidelines for the welfare of animals.

2.3. Blood sample collection

For administration of silica particles through an intravenous route, BALB/c mice were treated with nSP70, nSP300, mSP1000, nSP70-C, nSP70-N or saline at 0.8 mg/mouse. At various times (6 h, 24 h, 3 day and 7 day) after treatment of these silica particles, blood samples were collected. For administration of silica particles through an intranasal route, BALB/c mice were treated with nSP30, nSP70 or saline intranasally at 0.5 mg/mouse. Blood samples were collected 24 h after the treatment of these silica nanoparticles.

2.4. Analysis of biomarkers for nanomaterials using a proteomics approach

BALB/c mice were treated with 0.8 mg/mouse nSP70 or saline intravenously. After 24 h, blood samples were collected and plasma was harvested by centrifuging blood at 12000 rpm for 15 min. Proteo prep (Sigma–Aldrich; Saint Louis, MO) was used to remove albumin and immunoglobulins from the plasma according to the manufacturer's instructions. Plasma samples were then analyzed by sodium dodecyl sulfate-polyacrylamide gel electrophoresis (SDS-PAGE) followed by Coomassie Brilliant Blue staining. Plasma diluted into aliquots corresponding to 10 µg protein were mixed with an equal volume of Laemmli sample buffer (BIO-RAD, Tokyo, Japan) containing 5% 2-mercaptoethanol and boiled for 5 min prior to electrophoresis. Electrophoresis was performed at 15 mA for 10 min (stacking) followed by separation (600 V, 40 mA, 100 W) for approximately 45 min, using Precision Plus Protein Kaleidoscope molecular weight markers (BIO-RAD) as standards.

2.5. Identification of candidate proteins as biomarkers

Bands of interest were excised from the gel and then destained with 50% acetonitrile (ACN)/25 mM NH_4HCO_3 for 10 min, dehydrated with 100% ACN for 10 min, and then dried using a centrifugal concentrator. Next, 8 µl of 20 µl/ml trypsin solution (Promega, Madison, WI) diluted 5-fold in 50 mM NH_4HCO_3 was added to each gel piece and then incubated overnight at 37 °C. We used three solutions to extract the resulting peptide mixtures from the gel pieces. First, 50 µl of 50% (v/v) ACN in 0.1% aqueous trifluoroacetic acid (TFA) was added to the gel pieces, which were then sonicated for 30 min. Next, we collected the solution and added 80% (v/v) ACN in 0.1% TFA. Finally, 100% ACN was added for the last extraction. The peptide solution were dried and resuspended in 10 µl of 0.1% formic acid. The resulting peptide mixture was then analyzed by nano-flow liquid chromatography/tandem mass spectrometry (LC/MS; maXis, Bruker Daltonik GmbH, Bremen, Germany).

2.6. Measurement of acute phase proteins

Plasma levels of haptoglobin, C-reactive protein (CRP) and serum amyloid A (SAA) were measured by commercial enzyme-linked immunosorbent assay (ELISA) kits (Life Diagnostics, Inc.; West Chester, PA), according to the manufacturer's instructions.

2.7. Statistical analyses

All results are expressed as means \pm SD. Differences were compared by using the Bonferroni's method after analysis of variance (ANOVA).

3. Results

3.1. Identification of biomarkers of nanomaterials

We used silica particles as a model nanomaterial because it is one of the most common nanomaterials to have been developed. Silica particles are increasingly being used as additives in cosmetics and foods [17,18]. It is predicted that the global market for silica particles will soon grow to \$2 billion and a ton of silica particles is currently produced worldwide every year. Here, we used silica particles with a diameter of 30, 70, 300 and 1000 nm (nSP30, nSP70, nSP300 and mSP1000, respectively). The mean secondary particle diameters of the silica particles measured by Zetasizer were 33, 79, 326 and 945 nm, respectively (data not shown). The silica particles were confirmed to be well dispersed smooth-surfaced spheres by transmission electron microscopy (data not shown).

Initially, we attempted to identify protein biomarkers in mice by analyzing changes in the level of each plasma protein following treatment with silica nanoparticles using a proteomics approach. BALB/c mice were intravenously treated with nSP70 (0.8 mg/mouse) or saline and then plasma samples were collected 24 h later. Because albumin and immunoglobulins are known to account for the majority of plasma proteins, they were removed from the samples prior to analysis so that variation in the level of other proteins could be more closely monitored. The change of protein levels in plasma after treatment with nSP70 was assessed by SDS-PAGE analysis (Fig. 1). The intensity of a band of molecular mass 37 kDa was more intense in the plasma of nSP70 treated mice than that of saline treated control mice (Fig. 1). The band was excised and analyzed by LC/MS in order to identify the corresponding protein. This analysis identified the induced band after treatment with nSP70 as haptoglobin, one of the acute phase proteins.

3.2. The level of haptoglobin after treatment with silica particles

To assess the change of haptoglobin level in plasma after administration of silica particles, BALB/c mice were intravenously treated with nSP70, nSP300 or mSP1000 at 0.8 mg/mouse. We did not use nSP30 in the experiment, because nSP30 induced the toxic side effects after intravenous treatment at this dose. We confirmed that nSP70, nSP300 or mSP1000 at this dose did not induce any

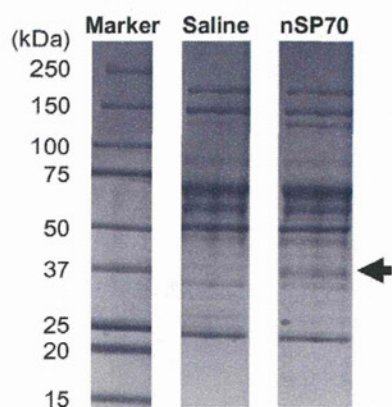


Fig. 1. SDS-PAGE analysis of plasma proteins. BALB/c mice were intravenously treated with nSP70 or saline at 0.8 mg/mouse. After 24 h, blood samples were collected. The change of protein levels in plasma after treatment of nSP70 was assessed by SDS-PAGE.

significant elevation of tissue injury and dysfunction markers such as alanine aminotransferase (ALT), aspartate aminotransferase (AST) and blood urea nitrogen (BUN) (data not shown). After 24 h, the level of haptoglobin in the plasma was analyzed by ELISA (Fig. 2A). The levels of haptoglobin in the plasma of nSP70 treated mice were significantly higher than those of saline treated control mice. In contrast, the levels of haptoglobin in the plasma of mSP1000 treated mice were almost the same as those of the saline treated control group. The haptoglobin levels of nSP300 treated mice were slightly higher than those of saline treated control mice. These results indicate that the levels of haptoglobin in the plasma of mice increase as the silica particle size decreases. Thus, haptoglobin appears to be a valuable biomarker for exposure to silica particles of nanometer size.

To assess the potential of haptoglobin as biomarker more precisely, we examined the sensitivity and time dependency of changes in haptoglobin level after treatment with silica particles. BALB/c mice were treated with nSP70, nSP300 or mSP1000 intravenously at 0.8 mg/mouse. After 6 h, 24 h, 3 day and 7 day, we examined the level of haptoglobin in the plasma by ELISA (Fig. 2B). No elevation of haptoglobin in the plasma of mSP1000 treated mice was observed. However, nSP70 and nSP300 treated mice showed a maximum level of haptoglobin 24 h after treatment. Furthermore, at 3 days after treatment, the level of haptoglobin in nSP70 treated mice was significantly higher than saline treated control mice. Next, BALB/c mice were treated with 0.2 and 0.05 mg/mouse nSP70 intravenously. After 24 h, we examined the level of haptoglobin in the plasma by ELISA (Fig. 2C). Mice treated with 0.2 and 0.05 mg/mouse nSP70 did not show any elevated level of haptoglobin. These results indicate that the level of haptoglobin is elevated as the particle size of silica particles decreases and that an increase of haptoglobin is dependent on the concentration of silica particles.

3.3. Response of other acute phase proteins

Haptoglobin, CRP and SAA are typical acute phase proteins that are induced during infection and inflammation [19]. To assess the levels of CRP and SAA in plasma after administration of silica particles, BALB/c mice were intravenously treated with nSP70, nSP300 or mSP1000 at 0.8 mg/mouse. After 6 h, 24 h, 3 day and 7 day, we examined the level of CRP (Fig. 3A) and SAA (Fig. 3B) in the plasma of the mice by ELISA. At 6 h and 24 h, both the level of CRP and SAA in the plasma of mice treated with nSP70 was significantly higher than those of the saline treated control mice. Furthermore, the maximum level of CRP in nSP70 treated mice was observed at

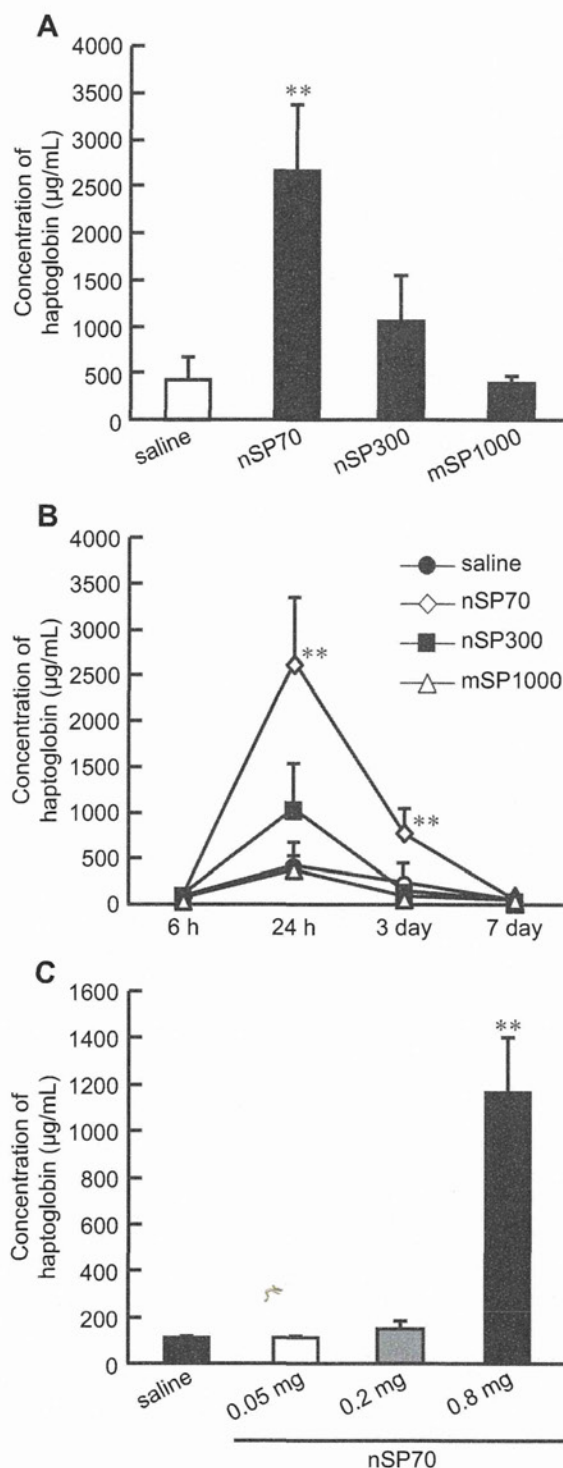


Fig. 2. The potential of haptoglobin as biomarker of nanomaterials. (A) The level of haptoglobin after treatment with silica particles. BALB/c mice were intravenously treated with nSP70, nSP300 or mSP1000 at 0.8 mg/mouse. After 24 h, the level of haptoglobin in the plasma of each mouse was examined by ELISA. (B) The time dependency of haptoglobin expression after treatment with silica particles. BALB/c mice were intravenously treated with nSP70, nSP300 or mSP1000 at 0.8 mg/mouse. After 6 h, 24 h, 3 day and 7 day, blood samples were collected. The level of haptoglobin in the plasma of the mice was determined by ELISA. (C) The sensitivity of haptoglobin after treatment of silica particles. BALB/c mice were intravenously treated with nSP70 at 0.8, 0.2 or 0.05 mg/mouse. After 24 h, blood samples were collected. The level of haptoglobin in the plasma of treated mice was determined by ELISA. Data are presented as mean \pm SD ($n = 5-6$; ** $P < 0.01$ versus value for saline treated group by ANOVA).

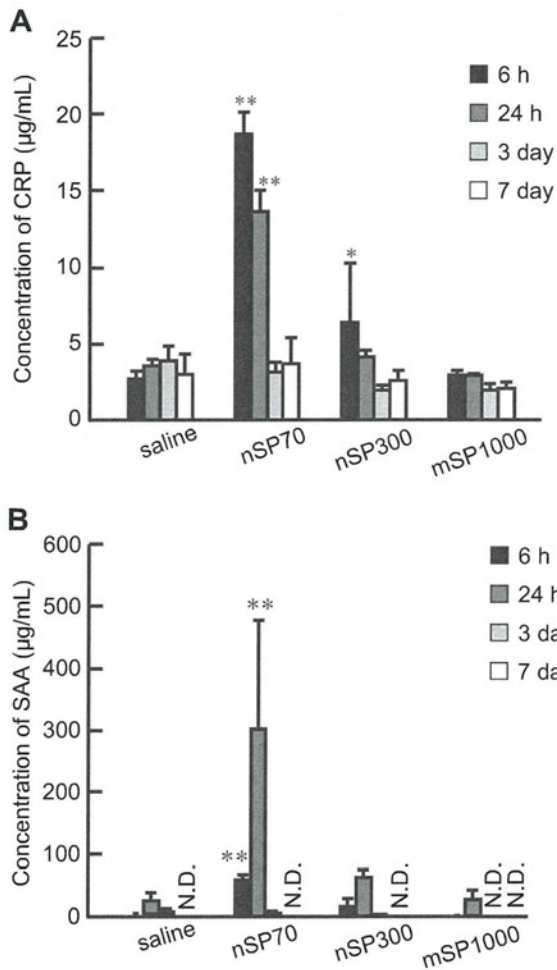


Fig. 3. Response of other acute phase proteins. BALB/c mice were intravenously treated with nSP70, nSP300 or mSP1000 at 0.8 mg/mouse. After 6 h, 24 h, 3 day and 7 day, blood samples were collected. The levels of (A) CRP and (B) SAA in the plasma of treated mice were examined by ELISA. Data are presented as mean \pm SD ($n = 5-6$; * $P < 0.05$, ** $P < 0.01$ versus value for saline treated group by ANOVA; N.D., not detected).

6 h after treatment, whereas that of haptoglobin and SAA was observed at 24 h. In contrast, the level of CRP and SAA in plasma of mSP1000 treated mice were almost the same as that of the saline treated control mice at all time points. The level of CRP in the plasma of nSP300 treated mice was slightly higher than that of saline treated control mice at 6 h. Our results suggest that both SAA and CRP may be useful biomarkers for predicting the risk from exposure to silica nanoparticles as well as haptoglobin. Indeed, these biomarkers could give even better response and sensitivity when used in combination.

3.4. The level of acute phase proteins through various routes

Exposure to nanomaterials in our daily lives can occur through various different routes. For example, nanomaterials contained in foods and drug medicines are taken up orally, whereas nanomaterials spread in the environment generally enter the body intranasally. Therefore, there is a need to evaluate suitable biomarkers for the exposure of nanomaterials through various routes. To assess the response of acute phase proteins to

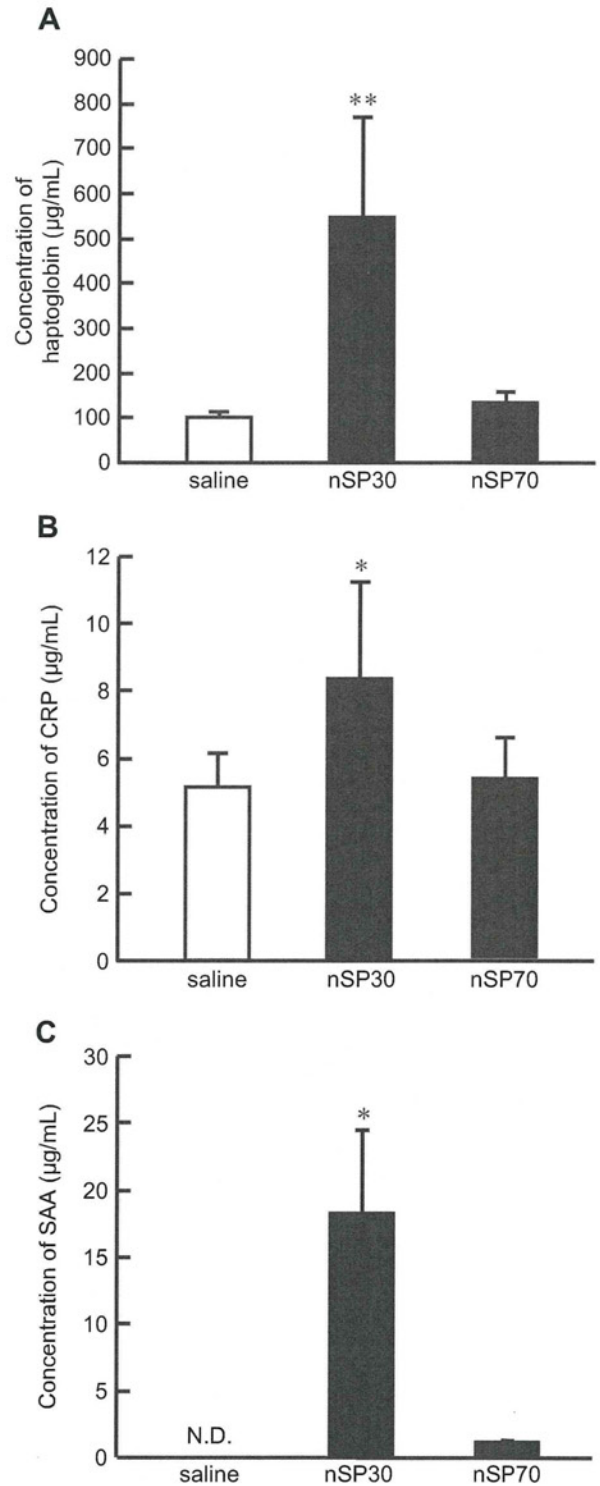


Fig. 4. Application of acute phase proteins to assess exposure of nanomaterials through various routes. To assess the administration of silica nanoparticles through an intranasal route, BALB/c mice were treated with nSP30, nSP70 or saline intranasally at 0.5 mg/mouse. Blood samples were collected 24 h after treatment. The level of (A) haptoglobin, (B) CRP and (C) SAA in the plasma were examined by ELISA. Data are presented as mean \pm SD ($n = 5-6$; * $P < 0.05$, ** $P < 0.01$ versus value for saline treated group by ANOVA; N.D., not detected).

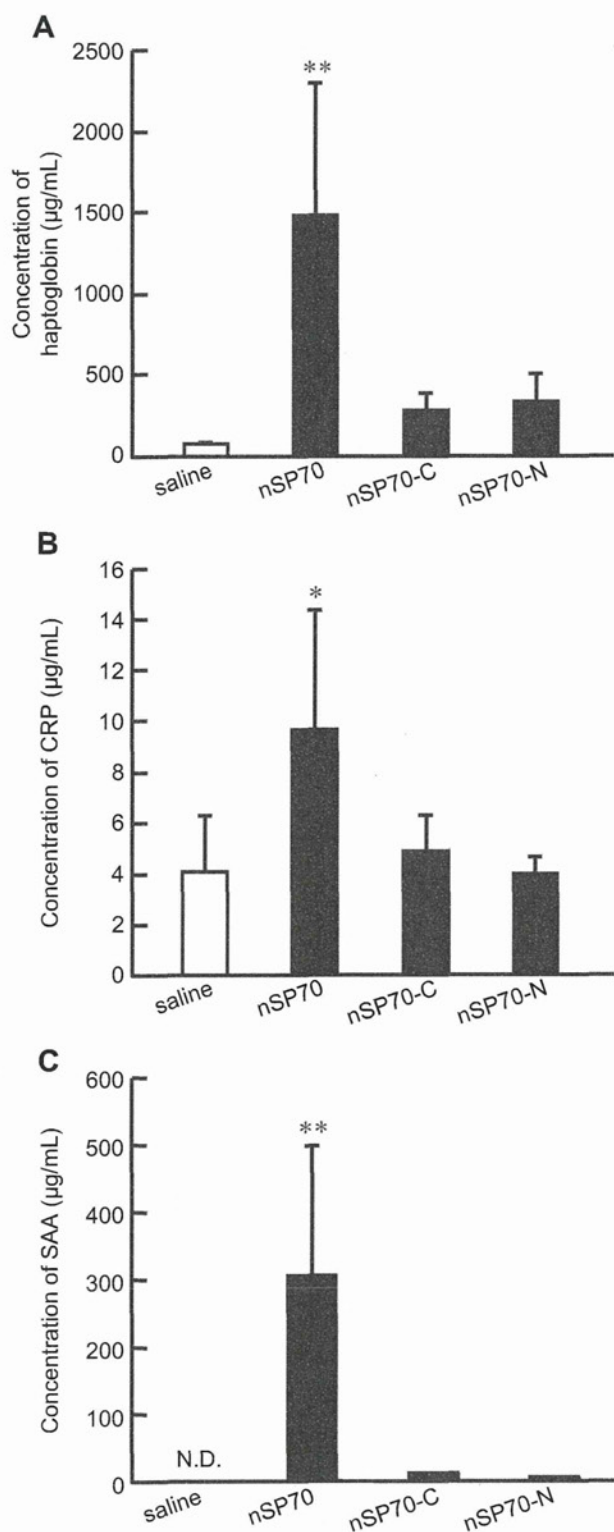


Fig. 5. Responses of acute phase proteins by the exposure to surface modified nSP70. BALB/c mice were intravenously treated with nSP70 modified with amino or carboxyl groups at 0.8 mg/mouse. After 24 h, the level of (A) haptoglobin, (B) CRP and (C) SAA in the plasma of treated mice were examined by ELISA. Data are presented as mean \pm SD ($n = 5-6$; * $P < 0.05$, ** $P < 0.01$ versus value for saline treated group by ANOVA; N.D., not detected).

silica particles introduced via different routes, we examined the level of haptoglobin, CRP and SAA in plasma after treatment of silica particles intranasally (Fig. 4). In this experiment, we used nSP30 and nSP70. For the administration of silica nanoparticles through an intranasal route, BALB/c mice were treated with nSP30, nSP70 or saline intranasally at 0.5 mg/mouse. After 24 h, we examined the level of haptoglobin (Fig. 4A), CRP (Fig. 4B) and SAA (Fig. 4C) in the plasma of the mice by ELISA. We showed that the level of haptoglobin, CRP and SAA in the plasma of mice treated with nSP30 intranasally was significantly higher than those of the saline treated control mice, although intranasal administration of nSP70 did not cause elevation in the plasma level of each acute phase protein in the treated mice. These results suggest that acute phase proteins could be useful biomarkers for predicting the risk arising from exposure to silica nanoparticles through various routes.

3.5. The level of acute phase proteins after treatment with surface modified silica nanoparticles

It has recently become evident that particle characteristics, including particle size and surface properties, are important factors in pathologic alterations and cellular responses [8,20–22]. Previously, our group also showed that surface modification of silica particles with functional groups such as amino or carboxyl group suppressed toxic biological effects of silica particles such as inflammatory responses [23]. To assess whether acute phase proteins could be useful biomarkers to predict risk factors associated with exposure to silica particles, we examined the level of haptoglobin (Fig. 5A), CRP (Fig. 5B) and SAA (Fig. 5C) in the plasma of mice after administration of nSP70 with amino or carboxyl group surface modifications. BALB/c mice were treated with 0.8 mg/mouse of these silica particles intravenously. After 24 h, we examined the level of haptoglobin, CRP and SAA in the plasma of the treated mice by ELISA. Our results showed that the level of these acute phase proteins in the plasma of nSP70 with amino or carboxyl group treated mice were significantly low compared with nSP70 treated mice.

4. Discussion

Our goal was to identify the biomarkers of nanomaterials for predicting their potential toxicity and to provide basic information for the creation of safe nanomaterials. To achieve these purposes, we tried to identify biomarkers in blood using a proteomics analysis. At first, we showed that the silica nanoparticles with small particle sizes (diameter < 100 nm) induced a higher level of acute phase proteins such as haptoglobin, CRP and SAA than larger silica particles (diameter > 100 nm) after intravenously treatment (Figs. 2 and 3). Previously, our group has shown that silica nanoparticles with relatively small particle size such as nSP70 induce a greater level of toxicity, including liver injury, compared to those of larger particle size [10,11]. Thus, there is a correlation between toxicity induced by the silica nanoparticles and the level of each potential plasma biomarker. Therefore, these acute phase proteins appear to be good biomarkers for predicting the strength of toxicity induced by silica nanoparticles.

The acute phase response is the nonspecific early response of an organism to infection and inflammation [24]. It comprises a whole array of systemic reactions and induction of a group of serum proteins called the acute phase proteins [25]. Monitoring the progression of infection and cancer by acute phase protein measurements in blood samples is used extensively in human patients. For example, haptoglobin is a biomarker of pancreatic cancer [26]. CRP is used as an index for the development of atrial fibrillation and maintenance [27], although mouse CRP is

synthesized only in trace amounts unlike its human counterpart [28]. In addition, both SAA and CRP are used as an index for adverse prognosis of breast cancer [29]. Therefore, we believe that these diagnostic systems using acute phase proteins for human health would be useful for predicting the risk of exposure to nanomaterials as well as their likely toxicities. In addition, we showed that the induction time for the maximum level of haptoglobin, SAA and CRP are different after treatment with the silica nanoparticles (Figs. 2 and 3). Therefore, the predictive quality of these biomarkers is improved when they are used in combination.

Epidemiological studies have suggested that increased levels of ambient particle including particle with nanometer size are associated with adverse effects in the respiratory and cardiovascular systems [30]. Some reports have shown that humans exposed to ambient particle have increased blood levels of CRP [31]. In addition, epidemiological studies have shown associations between increased concentrations of SAA and CRP in plasma, and increased risk of cardiovascular diseases [32] and cancer [33]. Therefore we consider that acute phase proteins would be biomarkers for predicting the risk of inflammatory disease, cardiovascular diseases and cancer after exposure by nanomaterials.

In recent years there has been increasing use of nanomaterials in cosmetics, due to their light-diffusing properties and absorbencies, as well as in foodstuffs, such as additives in powdered foods. In particular, silica particles have been extensively used in many consumer products. For example, in the US, the use of amorphous silica is limited to less than 2.0% by weight of common salt. Other limits are defined for finished foods (<1%) and dried egg products (<5%). We cannot avoid exposure to nanomaterials, either from the unintentional release of waste products into the environment or by exposure to medicines, cosmetics and foodstuffs. Thus, it is important to carry out a safety analysis of nanomaterials after exposure *via* various routes. In this study, we showed that the level of acute phase proteins in the plasma of mice treated with nSP30 intranasally was elevated, although nSP70 did not induce elevation of each acute phase protein (Fig. 4). Therefore we consider that nSP30 would induce any toxic biological effects after intranasally treatment. Now we are trying to examine the pharmacokinetics and biological effects of nSP30 after intranasally treatment.

We then examined the effects of surface modification of silica nanoparticles on the production of acute phase proteins, because it has become evident that surface properties are important factors in the biological effects of particles. We showed that nSP70 with amino or carboxyl group surface modifications did not induce the production of each acute phase proteins (Fig. 5). Previously, we showed that surface modification of silica particles with functional groups such as amino or carboxyl group suppressed toxic biological effects of silica particles such as inflammatory responses [23]. These results also suggest that acute phase proteins could be a promising candidate biomarker for predicting the strength of toxicity induced by silica nanoparticles, although it is need to examine the toxic biological effects of silica nanoparticles with functional groups. Over recent years, nanomaterials have been introduced into our everyday lives. For example, silica particles, titanium dioxide and fullerenes of various crystallographic structures and surface functional groups are used in a range of different consumer products. Therefore, we are now trying to evaluate the response of acute phase proteins to exposure from various nanomaterials.

In general, acute phase proteins are known to be released from the liver mainly as a result of inflammatory cytokines such as interleukin (IL)-6 [19]. However, we confirmed that the levels of IL-6 were not elevated in the plasma of mice treated with silica particles at 24 h after treatment (data not shown). Therefore it is unclear why nanomaterials induce the production of acute phase

proteins. We already showed that although silica particles with micrometer size tend to be taken up by Kupffer cells, silica nanoparticles with small particle sizes distribute around hepatic parenchymal cells (unpublished data). It is conceivable that instead of inflammatory cytokines, small silica particles act directly on the liver to induce the release of acute phase proteins. We are currently analyzing the detailed mechanism by which silica particles induce acute phase proteins in order to identify additional protein biomarkers.

5. Conclusions

We show here that acute phase proteins such as haptoglobin, CRP and SAA can act as useful biomarkers for analyzing the risk of exposure to nanomaterials and their associated toxicity. We believe that such information would be vital for the future development of predictive tests for estimation of the potential toxicity of new nanomaterials based on their physicochemical characteristics.

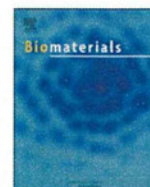
Acknowledgements

This study was supported in part by Grants-in-Aid for Scientific Research from the Ministry of Education, Culture, Sports, Science and Technology of Japan, and from the Japan Society for the Promotion of Science (JSPS). This study was also supported in part by Health Labour Sciences Research Grants from the Ministry of Health, Labor and Welfare of Japan; by Health Sciences Research Grants for Research on Publicly Essential Drugs and Medical Devices from the Japan Health Sciences Foundation; by a Global Environment Research Fund from Minister of the Environment; and by a the Knowledge Cluster Initiative; and by The Nagai Foundation Tokyo; and by The Cosmetology Research Foundation; and by The Smoking Research Foundation.

References

- [1] Rutherglen C, Burke P. Nanoelectromagnetics: circuit and electromagnetic properties of carbon nanotubes. *Small* 2009;5:884–906.
- [2] Kaur IP, Agrawal R. Nanotechnology: a new paradigm in cosmeceuticals. *Recent Pat Drug Deliv Formul* 2007;1:171–82.
- [3] Cormode DP, Jarzyna PA, Mulder WJ, Fayad ZA. Modified natural nanoparticles as contrast agents for medical imaging. *Adv Drug Deliv Rev* 2010;62:329–38.
- [4] Nel A, Xia T, Madler L, Li N. Toxic potential of materials at the nanolevel. *Science* 2006;311:622–7.
- [5] Donaldson K, Murphy FA, Duffin R, Poland CA. Asbestos, carbon nanotubes and the pleural mesothelium: a review of the hypothesis regarding the role of long fibre retention in the parietal pleura, inflammation and mesothelioma. *Part Fibre Toxicol* 2010;7:5.
- [6] Shvedova AA, Kagan VE, Fadeel B. Close encounters of the small kind: adverse effects of man-made materials interfacing with the nano-cosmos of biological systems. *Annu Rev Pharmacol Toxicol* 2010;50:63–88.
- [7] Poland CA, Duffin R, Kinloch I, Maynard A, Wallace WA, Seaton A, et al. Carbon nanotubes introduced into the abdominal cavity of mice show asbestos-like pathogenicity in a pilot study. *Nat Nanotechnol* 2008;3:423–8.
- [8] Morishige T, Yoshioka Y, Tanabe A, Yao X, Tsunoda S, Tsutsumi Y, et al. Titanium dioxide induces different levels of IL-1beta production dependent on its particle characteristics through caspase-1 activation mediated by reactive oxygen species and cathepsin B. *Biochem Biophys Res Commun* 2010;392:160–5.
- [9] Hougaard KS, Jackson P, Jensen KA, Sloth JJ, Loschner K, Larsen EH, et al. Effects of prenatal exposure to surface-coated nanosized titanium dioxide (UV-Titan). A study in mice. *Part Fibre Toxicol* 2010;7:16.
- [10] Nishimori H, Kondoh M, Isoda K, Tsunoda S, Tsutsumi Y, Yagi K. Silica nanoparticles as hepatotoxicants. *Eur J Pharm Biopharm* 2009;72:496–501.
- [11] Nishimori H, Kondoh M, Isoda K, Tsunoda S, Tsutsumi Y, Yagi K. Histological analysis of 70-nm silica particles-induced chronic toxicity in mice. *Eur J Pharm Biopharm* 2009;72:626–9.
- [12] Nishimori H, Kondoh M, Isoda K, Tsunoda S, Tsutsumi Y, Yagi K. Influence of 70 nm silica particles in mice with cisplatin or paraquat-induced toxicity. *Pharmazie* 2009;64:395–7.
- [13] Casado B, Iadarola P, Luisetti M, Kussmann M. Proteomics-based diagnosis of chronic obstructive pulmonary disease: the hunt for new markers. *Expert Rev Proteomics* 2008;5:693–704.

- [14] Ferte C, Andre F, Soria JC. Molecular circuits of solid tumors: prognostic and predictive tools for bedside use. *Nat Rev Clin Oncol*; 2010 Jun 15 [Epub ahead of print].
- [15] Vaidya VS, Ozer JS, Dieterle F, Collings FB, Ramirez V, Troth S, et al. Kidney injury molecule-1 outperforms traditional biomarkers of kidney injury in preclinical biomarker qualification studies. *Nat Biotechnol* 2010;28:478–85.
- [16] Ozer JS, Dieterle F, Troth S, Perentes E, Cordier A, Verdes P, et al. A panel of urinary biomarkers to monitor reversibility of renal injury and a serum marker with improved potential to assess renal function. *Nat Biotechnol* 2010;28:486–94.
- [17] Villota R, Hawkes JG. Food applications and the toxicological and nutritional implications of amorphous silicon dioxide. *Crit Rev Food Sci Nutr* 1986;23:289–321.
- [18] Merget R, Bauer T, Kupper HU, Philippou S, Bauer HD, Breitschadt R, et al. Health hazards due to the inhalation of amorphous silica. *Arch Toxicol* 2002;75:625–34.
- [19] Gabay C, Kushner I. Acute-phase proteins and other systemic responses to inflammation. *N Engl J Med* 1999;340:448–54.
- [20] He X, Nie H, Wang K, Tan W, Wu X, Zhang P. In vivo study of biodistribution and urinary excretion of surface-modified silica nanoparticles. *Anal Chem* 2008;80:9597–603.
- [21] Nabeshi H, Yoshikawa T, Matsuyama K, Nakazato Y, Arimori A, Isobe M, et al. Size-dependent cytotoxic effects of amorphous silica nanoparticles on Langerhans cells. *Pharmazie* 2010;65:199–201.
- [22] Yamashita K, Yoshioka Y, Higashisaka K, Morishita Y, Yoshida T, Fujimura M, et al. Carbon nanotubes elicit DNA damage and inflammatory response relative to their size and shape. *Inflammation* 2010;33:276–80.
- [23] Morishige T, Yoshioka Y, Inakura H, Tanabe A, Yao X, Narimatsu S, et al. The effect of surface modification of amorphous silica particles on NLRP3 inflammasome mediated IL-1 β production, ROS production and endosomal rupture. *Biomaterials*; 2010 Jun 17 [Epub ahead of print].
- [24] Baumann H, Gauldie J. The acute phase response. *Immunol Today* 1994;15:74–80.
- [25] Kushner I. The phenomenon of the acute phase response. *Ann N Y Acad Sci* 1982;389:39–48.
- [26] Firpo MA, Gay DZ, Granger SR, Scaife CL, DiSario JA, Boucher KM, et al. Improved diagnosis of pancreatic adenocarcinoma using haptoglobin and serum amyloid A in a panel screen. *World J Surg* 2009;33:716–22.
- [27] Korantzopoulos P, Kalantzi K, Siogas K, Goudevenos JA. Long-term prognostic value of baseline C-reactive protein in predicting recurrence of atrial fibrillation after electrical cardioversion. *Pacing Clin Electrophysiol* 2008;31:1272–6.
- [28] Szalai AJ, McCrory MA. Varied biologic functions of C-reactive protein: lessons learned from transgenic mice. *Immunol Res* 2002;26:279–87.
- [29] Pierce BL, Neuhaus ML, Wener MH, Bernstein L, Baumgartner RN, Ballard-Barbash R, et al. Correlates of circulating C-reactive protein and serum amyloid A concentrations in breast cancer survivors. *Breast Cancer Res Treat* 2009;114:155–67.
- [30] Mauderly JL, Chow JC. Health effects of organic aerosols. *Inhal Toxicol* 2008;20:257–88.
- [31] Ruckerl R, Ibaldo-Mulli A, Koenig W, Schneider A, Woelke G, Cyrys J, et al. Air pollution and markers of inflammation and coagulation in patients with coronary heart disease. *Am J Respir Crit Care Med* 2006;173:432–41.
- [32] Albert MA, Ridker PM. The role of C-reactive protein in cardiovascular disease risk. *Curr Cardiol Rep* 1999;1:99–104.
- [33] Siemes C, Visser LE, Coebergh JW, Splinter TA, Wittteman JC, Uitterlinden AG, et al. C-reactive protein levels, variation in the C-reactive protein gene, and cancer risk: the Rotterdam Study. *J Clin Oncol* 2006;24:5216–22.



Systemic distribution, nuclear entry and cytotoxicity of amorphous nanosilica following topical application

Hiromi Nabeshi^{a,b,1}, Tomoaki Yoshikawa^{a,b,1,*}, Keigo Matsuyama^{a,b}, Yasutaro Nakazato^{a,b}, Kazuhiko Matsuo^c, Akihiro Arimori^{a,b}, Masaaki Isobe^{a,b}, Saeko Tochigi^{a,b}, Sayuri Kondoh^{a,b}, Toshiro Hirai^{a,b}, Takanori Akase^{a,b}, Takuya Yamashita^{a,b}, Kohei Yamashita^{a,b}, Tokuyuki Yoshida^{a,b}, Kazuya Nagano^b, Yasuhiro Abe^b, Yasuo Yoshioka^{b,d}, Haruhiko Kamada^{b,d}, Takayoshi Imazawa^e, Norio Itoh^a, Shinsaku Nakagawa^c, Tadanori Mayumi^f, Shin-ichi Tsunoda^{b,g}, Yasuo Tsutsumi^{a,b,d,*}

^a Department of Toxicology and Safety Science, Graduate School of Pharmaceutical Sciences, Osaka University, 1-6 Yamadaoka, Suita, Osaka 565-0871, Japan

^b Laboratory of Biopharmaceutical Research (Pharmaceutical Proteomics), National Institute of Biomedical Innovation, 7-6-8 Saito-Asagi, Ibaraki, Osaka 567-0085, Japan

^c Department of Biotechnology and Therapeutics, Graduate School of Pharmaceutical Sciences, Osaka University, 1-6 Yamadaoka, Suita, Osaka 565-0871, Japan

^d The Center for Advanced Medical Engineering and Informatics, Osaka University, 1-6 Yamadaoka, Suita, Osaka 565-0871, Japan

^e Bioresources Research, Laboratory of Common Apparatus, National Institute of Biomedical Innovation, 7-6-8 Saito-Asagi, Ibaraki, Osaka 567-0085, Japan

^f Graduate School of Pharmaceutical Sciences, Kobe-Gakuin University, 1-1-3 Minatogima, Chuo-ku, Kobe, Hyogo 650-8586, Japan

^g Department of Biomedical Innovation, Graduate School of Pharmaceutical Sciences, Osaka University, 7-6-8 Saito-Asagi, Ibaraki, Osaka 567-0085, Japan

ARTICLE INFO

Article history:

Received 12 October 2010

Accepted 27 December 2010

Available online 22 January 2011

Keywords:

Nanoparticles

Silica

Transdermal penetration

Cytotoxicity

Mutagenicity

ABSTRACT

Currently, nanomaterials (NMs) with particle sizes below 100 nm have been successfully employed in various industrial applications in medicine, cosmetics and foods. On the other hand, NMs can also be problematic in terms of eliciting a toxicological effect by their small size. However, biological and/or cellular responses to NMs are often inconsistent and even contradictory. In addition, relationships among NMs physicochemical properties, absorbency, localization and biological responses are not yet well understood. In order to open new frontiers in medical, cosmetics and foods fields by the safer NMs, it is necessary to collect the information of the detailed properties of NMs and then, build the prediction system of NMs safety. The present study was designed to examine the skin penetration, cellular localization, and cytotoxic effects of the well-dispersed amorphous silica particles of diameters ranging from 70 nm to 1000 nm. Our results suggested that the well-dispersed amorphous nanosilica of particle size 70 nm (nSP70) penetrated the skin barrier and caused systemic exposure in mouse, and induced mutagenic activity *in vitro*. Our information indicated that further studies of relation between physicochemical properties and biological responses are needed for the development and the safer form of NMs.

© 2011 Elsevier Ltd. All rights reserved.

1. Introduction

A nanomaterial (NM) is defined as a substance that has at least one dimension of less than 100 nm in size. NMs can assume many different forms, such as tubes, rods, wires, spheres or particles. NMs have been widely used in consumer and industrial applications, such as medicine, cosmetics and foods, because they exhibit unique physicochemical properties and innovative functions [1]. However,

NMs can also be problematic in terms of eliciting a toxicological effect by their small size. For example, exposure of cells or animals to carbon nanotubes, titanium dioxide nanoparticles or silver nanoparticles can induce cytotoxicity and inflammation [2–14]. We have previously shown that nSPs display a different intracellular localization compared with submicron- and micro-sized silica particles, and induce a greater cytotoxic response [15]. Whereas other studies reported that carbon nanotubes and titanium dioxide nanoparticles do not induce harmful effects [16–18]. Thus, despite intensive research efforts, reports of biological and/or cellular responses to NMs are often inconsistent and even contradictory. In addition, relationships among NMs physicochemical properties, absorbency, localization and biological responses are not yet well understood. In order to ensure the safety of NMs and open new frontiers in biological fields by the use of NMs, it is necessary to

* Corresponding authors. Department of Toxicology and Safety science, Graduate School of Pharmaceutical Sciences, Osaka University, 1-6 Yamadaoka, Suita, Osaka 565-0871, Japan. Tel.: +81 6 6879 8230; fax: +81 6 6879 8234.

E-mail addresses: tomoaki@phs.osaka-u.ac.jp (T. Yoshikawa), ytsutsumi@phs.osaka-u.ac.jp (Y. Tsutsumi).

¹ These authors contributed equally to the work.

collect the information of the detailed properties of NMs from the point of view of biosafety and then, build comprehensive prediction system of NMs safety.

Accordingly, in this study, we evaluated the absorption properties and intracellular distribution of NMs, using typical NMs, amorphous nanosilica particles (nSP) and quantum dots (QD). nSP are one of the most widely applied NMs, and are used in cosmetics and food additives. nSPs and QD also have great potential for use as diagnostic imaging agents, gene delivery carriers and cancer therapies [19–23]; in addition, these NMs show overwhelmingly superior dispersibility as compared with carbon nanotubes, fullerene and nano-sized titanium dioxide (TiO₂). Thus, these NMs are ideally suited for determining how particle size influences the biodistribution and biological effects of NMs.

2. Materials and methods

2.1. Silica particles

Suspensions of fluorescent (red-F)-labeled amorphous silica particles (Micro-mod Partikeltechnologie GmbH) (25 mg/ml and 50 mg/ml) were used in this study; particle size diameters were 70, 300 and 1000 nm (designated as nSP70, nSP300 and mSP1000, respectively). Silica particles were used following 5 min sonication and 1 min vortex.

2.2. Quantum dots

Quantum dots (QD) with emission maxima at 565 nm were obtained from Invitrogen (Hayward, CA). They were sold as Qtracker® Non-targeted Quantum Dots (PEG). QD were used after 5 min sonication and 1 min vortex.

2.3. Animals

BALB/c mice (female, 6–8 weeks) were purchased from Japan SLC, Inc. Mice were housed in a ventilated animal room maintained at 20 ± 2 °C with a 12-h light/12-h dark cycle. Mice had free access to water and alfalfa-free forage (FR-2, Funabashi farm). The experimental protocols conformed to the ethical guidelines of the National Institute of Biomedical Innovation.

2.4. Cell culture

HaCaT human keratinocyte cell line was kindly provided by Dr. Inui, Osaka University. HaCaT cells were cultured in Dulbecco's modified Eagle's medium (D-MEM) supplemented with 10% heat-inactivated fetal bovine serum and 0.2 mM *n*-glutamine. The cells were grown in a humidified incubator at 37 °C (95% room air, 5% CO₂).

2.5. Physicochemical examinations of silica particles and QD

Silica particles and QD were diluted to 0.25 mg/ml (nSP70), 0.5 mg/ml (nSP300 and mSP1000) or 0.5 μm (QD) with PBS, respectively and the average particle size and zeta potential were measured using the Zetasizer Nano-ZS (Malvern Instruments Ltd). The mean size and the size distribution of silica particles were measured by dynamic light scattering method. The zeta potential was measured by laser Doppler electrophoresis. pH of each particles suspension were measured by ISFET-pH meter (SHINDENGEN, Japan). The size and shape of silica particles and QD were observed using transmission electron microscopy (TEM). Prior to TEM analysis, nSP70 were stained with 2% uranium acetate and QD were enhanced by silver using a standard AURION R-GENT SE-EM reagent and protocol.

2.6. Dermal administration of silica particles and transmission electron microscopy (TEM) analysis of skin, lymph node and liver

nSP70 (250 μg/ear/day) and QD (1.2 pmol/ear/day) suspension supplemented with 10% isopropyl myristate were applied to the inner side of both ears of BALB/c mice for 28 days. In both samples, the total number of particles applied over 28 days was 2.8 × 10¹³ particles. After 24 h of last administration, skin, lymph node and brain from each mouse were excised and fixed in 2.5% glutaraldehyde for 2 h. Then, small pieces of tissue sample were washed with phosphate buffer three times and post-fixed in sodium cacodylate-buffered 1.5% osmium tetroxide for 60 min at 4 °C, block stained in 0.5% uranyl acetate, dehydrated by dipping each of them through a series of ethanol solutions containing increasing concentration of ethanol, and embedded in Epon resin (TAAB). Ultrathin sections were stained with uranyl acetate and lead citrate (silica particles-treated samples) or AURION R-GENT SE-EM reagent (QD-treated samples). The stained samples were subsequently observed under a Hitachi electron microscope (H-7650).

2.7. Detection of apoptotic cells in the nSP70-applied mice skin (terminal deoxynucleotidyl transferase-mediated X-dUTP nick-end labeling (TUNEL) staining)

The TUNEL staining was performed on paraffin-embedded skin sections of 28-day application of nSP70. The skin was fixed in 10% neutral buffered formalin and then embedded in paraffin. Paraffin-embedded skin was sliced and placed on glass slides. DNA strand breaks, which are associated with the apoptotic response, were detected with an *in situ* Cell Death Detection Kit, TMR red (Roche) according to protocol of this kit. Deparaffinization and rehydration of the skin sections were carried out according to standard protocols. Then, the skin sections were incubated with proteinase K for 30 min. After rinse of the skin sections twice with PBS, 50 μl of TUNEL reaction mixture were added on the skin sections and incubated for 60 min at 37 °C in the dark. The skin sections were rinsed 3 times with PBS and mounted with the mounting agent, ProLong Gold Antifade Reagent with DAPI (Invitrogen). The skin sections were analyzed under a fluorescence microscope (BIOREVO, KEYENCE) with excitation wavelength in the range of 520–560 nm and detection in the range of 570–620 nm. For counting the numbers of TUNEL-positive cells, approximately 1000 cells were randomly selected from 3 different areas in each section and examined under a fluorescence microscope at magnification of ×200.

2.8. Transmission electron microscopy (TEM) analysis of human keratinocyte cells

HaCaT cells were cultured in the presence of various sized silica particles (100 μg/ml) for 24 h on chamber slides, and then fixed in 2.5% glutaraldehyde followed by 1.5% osmium tetroxide. The fixed cells were dehydrated and embedded in EPON resin. Ultrathin sections were stained with lead citrate and observed under an electron microscope.

2.9. Evaluation of the proliferation of silica particle- or QD-treated cells (³H-thymidine incorporation assay)

Proliferation of silica particle- or QD-treated HaCaT cells was measured by ³H-thymidine incorporation assay. 1 × 10⁴ cells were cultured with varying concentrations of silica particles or QDs for 18 h at 37 °C and ³H-thymidine (1 μCi/well) was then added into each well. After a further 6 h, cells were harvested and lysed on glass fiber filter plates using a Cell harvester (PerkinElmer). The filter plates were then dried and counted by standard liquid scintillation counting techniques in a Top-Counter (PerkinElmer).

2.10. Mutagenicity assay (Ames test)

The mutagenicity assay was performed to evaluate the intrinsic mutagenic potency of the silica particles. For this purpose, the *Salmonella typhimurium* (*S. typhimurium*) mutagenicity test was performed according to the method of Ames [24–26]. Two strains of *S. typhimurium* bacteria were used, namely, TA98 and TA100. Experiments were conducted according to guideline of Health, Labour and Welfare Ministry. The test was carried out using 100 μl of well-dispersed solutions (10, 90, and 810 μg/ml) of silica particles. 2-Aminofluorene (2-AF) dissolved in DMSO was used as a positive control for the mutagenicity assay.

2.11. Determination of DNA damage (comet assay)

Damage of endogenous DNA in HaCaT cells after treatment with a given silica particles were analyzed by alkaline comet assay according to the Comet Assay Kit (Trevigen). All steps were conducted under dim yellow light to prevent additional DNA damage. Briefly, 3 × 10⁴ HaCaT cells were seeded into each well of a 6-well plate and incubated for 24 h. After 24 h, cells were treated with 30 or 90 μg/ml nSP70, nSP300, mSP1000 or 0.2 mM H₂O₂ (positive control) or PBS (negative control) for 3 h. Cells from each group were resuspended at a density of 1 × 10⁵ cells/ml in ice cold CMF-PBS and combined with molten LM Agarose (Trevigen) at a ratio of 1:10 (v/v). The cell-agarose mixture was immediately pipetted onto a frosted microscope slide (CometSlide; Trevigen). Each slide was then placed flat at 4 °C in the dark for 60 min, immersed in prechilled lysis solution (Trevigen), and left at 4 °C for 40 min to remove cellular proteins, leaving the DNA molecules exposed. The slides were then immersed in an alkaline solution (pH > 13, 0.3 M NaOH and 1 mM EDTA) for 40 min to denature the DNA and hydrolyze the sites that were damaged. The samples were electrophoresed for 10 min and stained with SYBR green I (Trevigen) according to the manufacturers instructions. Twenty-five cells on each slide, randomly selected by fluorescence microscopy, were then analyzed using the Comet Analyzer (Youworks Corporation).

2.12. In vivo imaging

Biodistribution of fluorescent-labeled silica particles was analyzed in live mice and excised tissues using the IVIS 200 imaging system (Xenogen corp.). Three female Hos: HR-1 mice were treated with 100 mg/kg DY-676 (excitation (ex) and emission (em) wavelengths 674 and 699 nm, respectively)-labeled silica particles of each particle size (70, 300 and 1000 nm) by intravenous injection. After anesthesia with isoflurane, live mouse fluorescence optical imaging was performed using the cy5.5